

PROMPT FISSION NEUTRON SPECTRA OF $^{233}\text{U}(n,F)$

V. M. Maslov¹

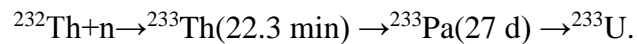
¹220025 Minsk, Byelorussia

¹E-mail: mvm2386@yandex.ru

Prompt fission neutron spectra (PFNS) are produced for incident neutron energies from thermal up to 20 MeV. Simultaneous analysis of measured and calculated data for $^{233}\text{U}(n,F)$, $^{235}\text{U}(n,F)$ and $^{239}\text{Pu}(n,F)$ maintains stronger justification for the predicted PFNS of $^{233}\text{U}(n,F)$. For the latter the reliable measured PFNS data are available at $E_n \sim E_{th}$ only. Pre-fission neutron spectra influence the partitioning of fission energy between excitation energy and total kinetic energy of fission fragments. For the reactions $^{233}\text{U}(n,F)$ and $^{235}\text{U}(n,F)$ we have shown that the shape of prompt fission neutron spectra (PFNS) depends on the fissility of composite and residual nuclides. The correlation of these peculiarities with emissive fission contributions (n,xf) to the observed fission cross section and competition of the reactions ($n,n\gamma$) and (n,xn)^{1...x} is established. Exclusive neutron spectra (n,xf)^{1...x} are consistent with fission cross sections of $^{235}\text{U}(n,F)$, $^{234}\text{U}(n,F)$, $^{233}\text{U}(n,F)$ and $^{232}\text{U}(n,F)$ reactions, as well as neutron emissive spectra of $^{235}\text{U}(n,xn)$ at ~ 14 MeV. Initial model parameters for $^{233}\text{U}(n,F)$ PFNS are fixed by description of PFNS of $^{233}\text{U}(n_{th},F)$. We predict the $^{233}\text{U}(n,xf)$ ^{1...x} exclusive pre-fission neutron spectra, exclusive neutron spectra of $^{233}\text{U}(n,xn)$ ^{1...x} reactions, total kinetic energy TKE of fission fragments and products, partials of average prompt fission neutron number and observed PFNS of $^{233}\text{U}(n,F)$. PFNS of $^{233}\text{U}(n,F)$ are harder than those of $^{235}\text{U}(n,F)$ PFNS, but softer than those of $^{239}\text{Pu}(n,F)$. Difference of average energies of PFNS $\langle E \rangle$ of $^{233}\text{U}(n,F)$ and $^{235}\text{U}(n,F)$ amounts to 1~3 %. At incident energies higher than ($n,2nf$) reaction threshold the observed PFNS may seem similar, though the partial contributions of $^{233}\text{U}(n,xf)$ and $^{235}\text{U}(n,xf)$ to the observed PFNS are quite different. Prompt fission neutron spectra (PFNS) of $^{233}\text{U}(n,F)$ are obtained in the energy range of $E_n \sim E_{th} - 20$ MeV, E_{th} being the thermal neutron energy. Consistent analysis of measured and theoretical data on PFNS for $^{233}\text{U}(n,F)$, $^{235}\text{U}(n,F)$ и $^{239}\text{Pu}(n,F)$ reactions.

1. Introduction

Fissile nuclide ^{233}U accumulates in breeder or hybrid reactor via reaction chains



$^{233}\text{U}+n$ nuclear data, with the exception for fission cross section, are scarce, especially as regards prompt fission neutron spectra $S(\varepsilon, E_n)$ of $^{233}\text{U}(n,F)$ in the excitation energy range where exclusive neutron spectra $^{233}\text{U}(n,xf)$ ^{1...x} emerge. Prompt fission neutron spectra $S(\varepsilon, E_n)$ measured at $E_n \sim 14.3$ MeV [1] remained the only available before long. Prompt fission neutron spectra in [1] were registered in a narrow energy range of $\varepsilon \sim 0.4 - 5$ MeV, however the excess of soft pre-fission neutrons in $S(\varepsilon, E_n)$ at $\varepsilon \sim 0.4 - 2$ MeV was observed. Afterwards it was described with a superposition of Weisskopf [2] and Watt [3] distributions:

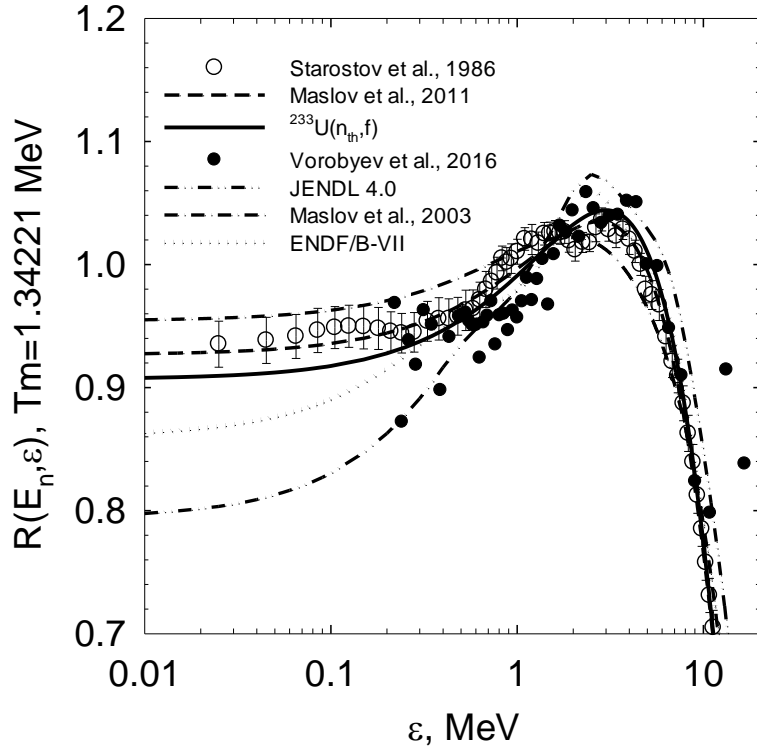


Fig.1. Prompt fission neutron spectra of $^{233}\text{U}(n_{\text{th}}, f)$ relative to Maxwellian-type distribution with $\langle E \rangle = 2,0564$ MeV: — $^{233}\text{U}(n_{\text{th}}, f)$; —•— [4, 5]; — — — [10]; ... — [16]; —••— [17]; ○ — [6]; ● — [8].

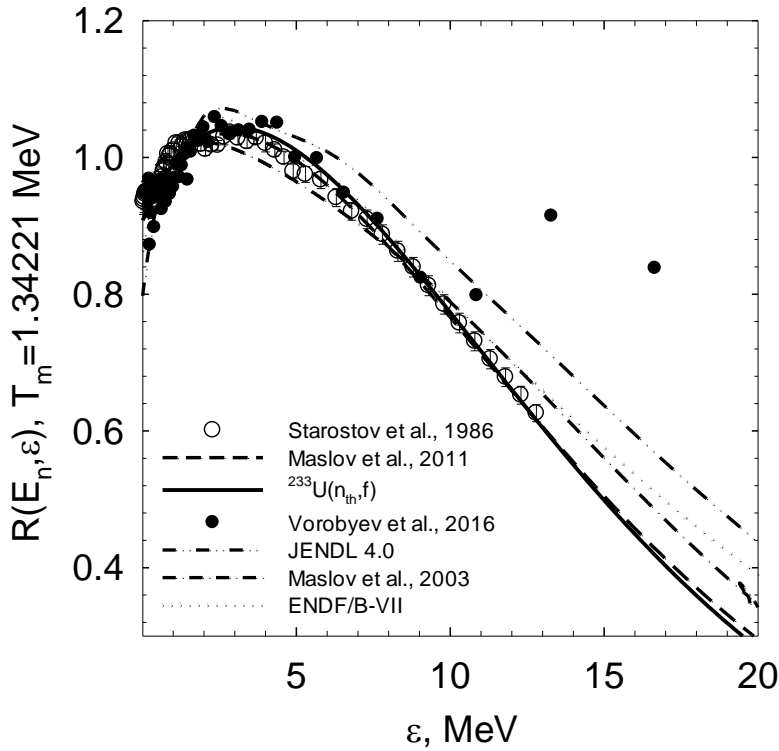


Fig.2. Prompt fission neutron spectra of $^{233}\text{U}(n_{\text{th}}, f)$ relative to Maxwellian-type distribution with $\langle E \rangle = 2,0564$ MeV: — $^{233}\text{U}(n_{\text{th}}, f)$; —•— [4, 5]; — — — [10]; ... — [16]; —••— [17]; ○ — [6]; ● — [8].

$$S(\varepsilon, E_n) = (1 - \beta)\varepsilon \exp\left(-\frac{\varepsilon}{T}\right) + \beta \exp\left(-\frac{\varepsilon}{T_f}\right) \frac{sh(2\sqrt{\omega\varepsilon})}{T_f}, \quad (1)$$

here $\beta=0.75$ – value of lumped contribution of post-fission neutrons, emitted from fission fragments, parameter $\omega=0.5$ MeV, average temperature of residual nuclide $T=0.55$ MeV, fission fragments temperature $T_f=1.2$ MeV. Since Eq.(1) is over-simplified, and energy range of $\varepsilon\sim 0.4\text{--}5$ MeV is rather narrow, relative contributions of pre- and post-fission neutrons of [1] disagree with newer research [4, 5]. However, the shape of calculated PFNS [1] looks similar to that of [4, 5]. Available measured data at $E_n\sim E_{th}$ [6] and $E_n\sim 0.55$ MeV [7], and data [1] as well, were abandoned in numerous versions of ENDF/B, JEFF and JENDL data libraries. The data of recent PFNS measurements $^{233}\text{U}(n_{th},f)$ [8], $^{235}\text{U}(n_{th},f)$ and $^{239}\text{Pu}(n_{th},f)$ [8, 9] are quite different as compared with data of [6]. Lumping [8, 9] data within spline fitting [10] would change PFNS shapes of $^{233}\text{U}(n_{th},f)$, $^{235}\text{U}(n_{th},f)$ and $^{239}\text{Pu}(n_{th},f)$ drastically (Fig. 1 and Fig. 2).

Differential PFNS data for target nuclides ^{235}U and ^{239}Pu are now available for incident neutron energies $E_n\sim 1.5\text{--}20$ MeV and outgoing neutron energies $\varepsilon\sim 0.01\text{--}10$ MeV [11–13]. In data of [11–13] strong variations of average energies of prompt fission neutrons $\langle E \rangle$ in the vicinity of (n,xf) reaction thresholds was observed. Average energies of prompt fission neutrons $\langle E \rangle$ are rough signature of PFNS, however it was established in [11–13] that the relative amplitude of $\langle E \rangle$ variation in case of $^{239}\text{Pu}(n,F)$ reaction is much weaker than in case of PFNS $\langle E \rangle$ of $^{235}\text{U}(n,F)$. That is obviously due to influence of (n,xf) fission channels on fission observables while emission of prompt fission neutrons is preceded by pre-fission neutrons. In case of $^{233}\text{U}(n,F)$ reactions similar variations of $\langle E \rangle$ were predicted in [4, 5, 10], they correlate with PFNS shape. Variations of $\langle E \rangle$ for $^{233}\text{U}(n,F)$ in ENDF/B–VII [14] are due to arbitrary and forced variation of PFNS shape to reproduce some assumed dependence of $\langle E \rangle(E_n)$. The ^{233}U data file of ENDF/B–VII [14], is borrowed by JEFF–3.3 [15] with some possible exceptions. In the version ENDF/B–VIII.0 [16] they adopted JENDL–4.0 [17]. In ROSFOND library [18] they use ^{233}U data file of [4, 5]. In BROND [19] prompt fission neutron spectra of ^{233}U [4, 5] are adopted, however that is a bit controversial procedure, since PFNS shape depends on the calculated $^{233}\text{U}+n$ data.

We intend to define/predict PFNS of $^{233}\text{U}(n,F)$ reaction in the energy range $E_n\sim E_{th}\text{--}20$ MeV. For that purpose would be used methods proved by $^{239}\text{Pu}(n,F)$ and $^{235}\text{U}(n,F)$ PFNS data analysis and prediction.

2. Prompt fission neutrons

It follows from the $^{233}\text{U}(n_{th},f)$ PFNS data [8] analysis that in the energy range $0.02<\varepsilon<5$ MeV they support the evaluations of ENDF/B–VII [14] and JENDL–4.0 [17], while both evaluated PFNS disagree with data [6]. Data [6] are presented as spline approximation [10], which summons empirical features of consistent analysis [6] of $^{233}\text{U}(n_{th},f)$, $^{235}\text{U}(n_{th},f)$, $^{239}\text{Pu}(n_{th},f)$ and $^{252}\text{Cf}(sf)$ measured PFNS. In the outgoing neutron energy range $5<\varepsilon<11$ MeV

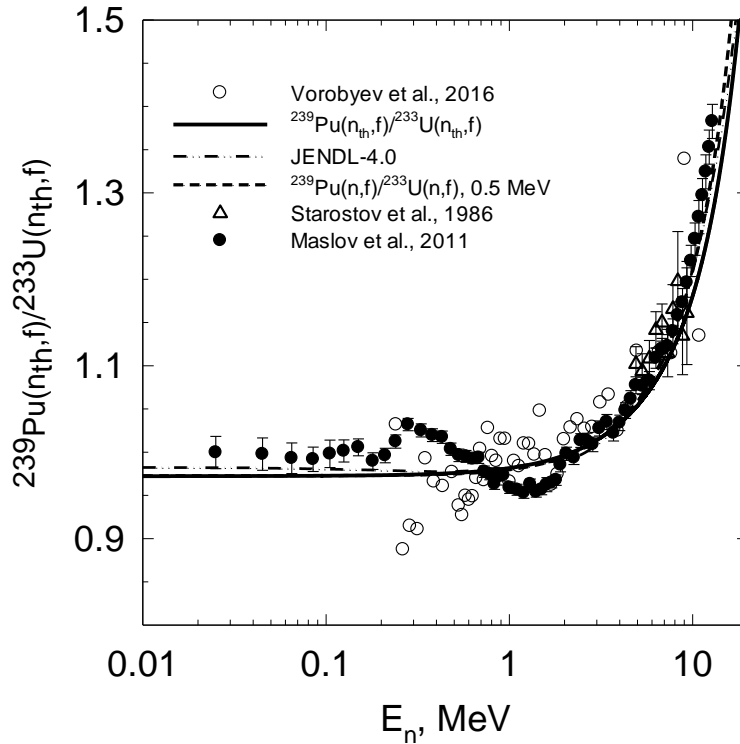


Fig.3. Ratio of PFNS of $^{239}\text{Pu}(n_{\text{th}},f)$ and $^{233}\text{U}(n_{\text{th}},f)$ for thermal neutron-induced fission: Δ — [6]; \circ — [8]; \bullet — [10]; — — present; —••— — [17]; — — — — $E_n = 0.5$ MeV.

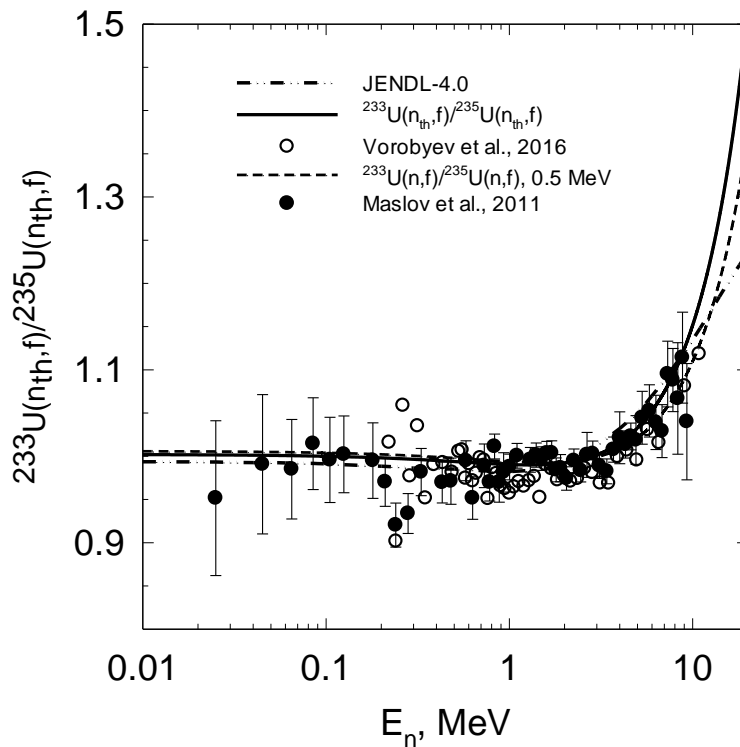


Fig.4. Ratio of PFNS of $^{233}\text{U}(n_{\text{th}},f)$ (n_{th},f) and $^{235}\text{U}(n_{\text{th}},f)$ for thermal neutron-induced fission: \circ — [8]; \bullet — [10]; — — present; —••— — [17]; — — — — $E_n = 0.5$ MeV.

data of [8] for $^{233}\text{U}(n,f)$ support the evaluation of [10], which encompasses data [6] in the energy range $0.02 < \varepsilon < 9.3$ MeV. The shape of $^{233}\text{U}(n_{th},f)$ PFNS of ENDF/B–VII [14] conforms with PFNS of $^{235}\text{U}(n_{th},f)$. It is well known that $^{235}\text{U}(n_{th},f)$ PFNS of ENDF/B–VII [14] only poorly describes measured data [20] at $E_n \sim 0.5$ MeV and disagree with newest measured data [11–13]. Moreover in ENDF/B–VIII [16], JEFF–3.3 [15] and JENDL–4.0 [17] at $E_n \sim E_{th}$ the JENDL–3.3 [18] evaluated data are used, which are uncorrelated with PFNS values at higher incident neutron energies $E_n > E_{th}$.

The comparison of PFNS measured data [6, 8, 9, 11–13] for $^{233}\text{U}(n, f)$, $^{235}\text{U}(n, f)$ и $^{239}\text{Pu}(n, f)$ in the energy range $E_{th} < E_n < E_{nff}$ shows that enhanced soft neutron yield, $\varepsilon \lesssim 1$ MeV, is a common feature except PFNS measured data [8, 9] at $E_n = E_{th}$ (see Fig. 1 and Fig. 2). In [8, 9] PFNS of $^{233}\text{U}(n_{th},f)$, $^{235}\text{U}(n,f)$ and $^{239}\text{Pu}(n,f)$ were measured relative to spontaneous fission neutron spectra of $^{252}\text{Cf}(sf)$. Afterwards various correction were applied to get absolute PFNS values, a number of systematic errors/uncertainties may appear, while the uncorrected ratios of various $^{233}\text{U}(n_{th},f)$, $^{235}\text{U}(n_{th},f)$ and $^{239}\text{Pu}(n_{th},f)$ PFNS pairs might be quite sterile in that respect.

The ratios of PFNS of $^{239}\text{Pu}(n_{th},f)/^{233}\text{U}(n_{th},f)$ and $^{233}\text{U}(n_{th},f)/^{235}\text{U}(n_{th},f)$ PFNS [8, 9] and [6], in the contrary to absolute PFNS of $^{233}\text{U}(n_{th},f)$, $^{235}\text{U}(n_{th},f)$ and $^{239}\text{Pu}(n_{th},f)$, quite agree with each other (see Fig. 3 and Fig. 4). Uncorrected PFNS data [6, 8, 9] are unavailable at the moment, though it would be preferable to compare their ratios. Figures 3 and 4 demonstrate that in the energy range $0.01 < \varepsilon < 10$ MeV the ratios of calculated PFNS of $^{239}\text{Pu}(n,f)$ and $^{235}\text{U}(n,f)$ at $E_n \sim E_{th}$ and $E_n \sim 0.5$ MeV only weakly depend on the incident neutron energy E_n . Calculated PFNS ratios of [4, 5, 10, 23], as well as present calculation, at $E_n \sim E_{th}$ and $E_n \sim 0.5$ MeV almost coincide with measured PFNS ratios $^{239}\text{Pu}(n_{th},f)/^{233}\text{U}(n_{th},f)$ and $^{233}\text{U}(n_{th},f)/^{235}\text{U}(n_{th},f)$ [6, 8, 9]. PFNS of JENDL–4.0 [17] contradict measured PFNS ratio $^{233}\text{U}(n,f)/^{235}\text{U}(n,f)$ at $E_n \sim E_{th}$. Similar contradiction happens in case of absolute PFNS values (see Fig. 5 and Fig. 6) Calculated PFNS at $E_n \sim 0.5$ MeV are compared with measured data $^{233}\text{U}(n,f)$, $^{235}\text{U}(n,f)$ [12, 22–24] and $^{239}\text{Pu}(n,f)$ [6, 13, 22]. It might be concluded that (see Figs. 3, 4, 5, 6) the harder neutrons are emitted in $^{239}\text{Pu}(n_{th},f)$ reaction, while the softest PFNS is that of $^{235}\text{U}(n_{th},f)$, PFNS of $^{233}\text{U}(n_{th},f)$ takes intermediate position.

At $E_n \sim 0.5$ and $E_n \sim 1.9$ MeV calculated/evaluated data deviate from measured data [7] in the energy range $\varepsilon > E_n$. Currently, at $E_n \sim E_{th}$ renormalization of model parameters after fitting data on total kinetic energy of fission fragments amounts to rather small changes of PFNS: for $^{239}\text{Pu}(n, f)$ decrease by $\sim 2\text{--}3\%$ at $\varepsilon < 1$ MeV, for $^{235}\text{U}(n, f)$ and $^{233}\text{U}(n,f)$ PFNS shifts by $\sim 1\text{--}2\%$ [24].

Pre–fission neutrons accompanying fission reaction when the incident neutron energy is higher than threshold of (n,nf) reaction, E_{nff} , influence the observed PFNS $S(\varepsilon, E_n)$ shape, total kinetic energy of fission fragments E_F^{pre} and fission products E_F^{post} , prompt fission neutron number $\nu_p(E_n)$, mass distributions and other fission observables.

Prompt fission neutron spectra $S(\varepsilon, E_n, \theta)$ at angle θ relative to the incident neutron beam, is a superposition of exclusive spectra of pre-fission neutrons, $(n,nf)^1$, $(n,2nf)^{1,2}$,

$(n,3nf)^{1,2,3} - \frac{d^2\sigma_{nxf}^k(\varepsilon, E_n, \theta)}{d\varepsilon d\theta}$ ($x=1, 2, 3; k=1, \dots, x$), and spectra of prompt fission neutrons, emitted by fission fragments, $S_{A+1-x}(\varepsilon, E_n, \theta)$:

$$\begin{aligned}
S(\varepsilon, E_n, \theta) &= \tilde{S}_{A+1}(\varepsilon, E_n, \theta) + \tilde{S}_A(\varepsilon, E_n, \theta) + \tilde{S}_{A-1}(\varepsilon, E_n, \theta) + \tilde{S}_{A-2}(\varepsilon, E_n, \theta) = \\
&\nu_p^{-1}(E_n, \theta) \cdot \left\{ \nu_{p1}(E_n) \cdot \beta_1(E_n, \theta) S_{A+1}(\varepsilon, E_n, \theta) + \nu_{p2}(E_n - \langle E_{nxf}(\theta) \rangle) \beta_2(E_n, \theta) S_A(\varepsilon, E_n, \theta) + \right. \\
&\beta_2(E_n, \theta) \frac{d^2\sigma_{nxf}^1(\varepsilon, E_n, \theta)}{d\varepsilon d\theta} + \nu_{p3}(E_n - B_n^A - \langle E_{n2nf}^1(\theta) \rangle - \langle E_{n2nf}^2(\theta) \rangle) \beta_3(E_n, \theta) S_{A-1}(\varepsilon, E_n, \theta) + \beta_3(E_n, \theta) \times \\
&\left[\frac{d^2\sigma_{n2nf}^1(\varepsilon, E_n, \theta)}{d\varepsilon d\theta} + \frac{d^2\sigma_{n2nf}^2(\varepsilon, E_n, \theta)}{d\varepsilon d\theta} \right] + \nu_{p4}(E_n - B_n^A - B_n^{A-1} - \langle E_{n3nf}^1(\theta) \rangle - \langle E_{n3nf}^2(\theta) \rangle - \langle E_{n3nf}^3(\theta) \rangle) \times \\
&\left. \beta_4(E_n, \theta) S_{A-2}(\varepsilon, E_n, \theta) + \beta_4(E_n, \theta) \left[\frac{d^2\sigma_{n3nf}^1(\varepsilon, E_n, \theta)}{d\varepsilon d\theta} + \frac{d^2\sigma_{n3nf}^2(\varepsilon, E_n, \theta)}{d\varepsilon d\theta} + \frac{d^2\sigma_{n3nf}^3(\varepsilon, E_n, \theta)}{d\varepsilon d\theta} \right] \right\}.
\end{aligned} \tag{2}$$

In equation (2) $\tilde{S}_{A+1-x}(\varepsilon, E_n, \theta)$ is the contribution of x -chance fission to the observed PFNS $S(\varepsilon, E_n, \theta)$, $\langle E_{nxf}^k(\theta) \rangle$ – average energy of k -th exclusive pre-fission neutron of (n, xnf) reaction with spectrum $\frac{d^2\sigma_{nxf}^k(\varepsilon, E_n, \theta)}{d\varepsilon d\theta}$, $k \leq x$. Spectra $S(\varepsilon, E_n, \theta)$, $S_{A+1-x}(\varepsilon, E_n, \theta)$ and $\frac{d^2\sigma_{nxf}^k(\varepsilon, E_n, \theta)}{d\varepsilon d\theta}$ are normalized to unity. Index x denotes the fission chance of $^{234-x}\text{U}$ after emission of x pre-fission neutrons, $\beta_x(E_n, \theta) = \sigma_{n,xf}(E_n, \theta) / \sigma_{n,F}(E_n, \theta)$ – contribution of x -th fission chance to the observed fission cross section, $\nu_p(E_n, \theta)$ is the observed average number of prompt fission neutrons, $\nu_{px}(E_{nx})$ – average number of prompt fission neutrons, emitted by $^{234-x}\text{U}$ nuclides. Spectra of prompt fission neutrons, emitted from fragments, $S_{A+2-x}(\varepsilon, E_n, \theta)$, as proposed in [24], were approximated by the sum of two Watt [3] distributions with different temperatures, relevant to the light and heavy fragments, the temperature of light fragment being higher.

Neutrons, evaporated by fission fragments $S_{A+1-x}(\varepsilon, E_n)$, as proposed in [24], are represented as a sum of two Watt distributions [3], resembling light and heavy fragments:

$$S_{A+1-x}(\varepsilon, E_n) = 0.5 \cdot \sum_{j=1}^2 W_j(\varepsilon, E_n, T_{xj}(E_n), \alpha), \tag{3}$$

$$W_j(\varepsilon, E_n, T_{xj}(E_n), \alpha) = \frac{2}{\sqrt{\pi} T_{xj}^{3/2}} \sqrt{\varepsilon} \exp\left(-\frac{\varepsilon}{T_{xj}}\right) \exp\left(-\frac{E_{vij}}{T_{xj}}\right) \frac{sh(\sqrt{b_{xj}\varepsilon})}{\sqrt{b_{xj}\varepsilon}}, \tag{4}$$

$$b_{xj} = \frac{4E_{vij}^0}{T_{xj}^2}, \quad T_{xj} = k_{xj} \sqrt{E_i^*} = k_{xj} \sqrt{E_r - E_{fx}^{pre} + U_x}. \tag{5}$$

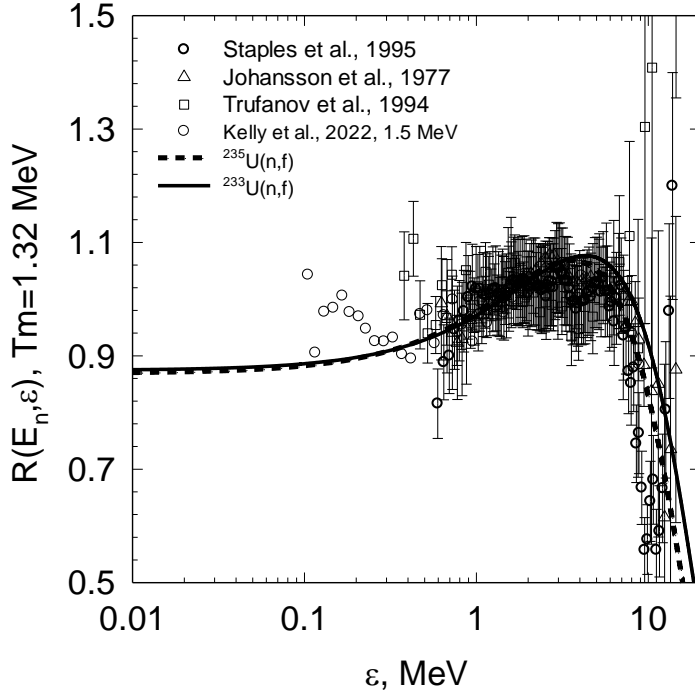


Fig.5 Prompt fission neutron spectra at $E_n = 0.5$ MeV relative to Maxwellian-type distribution with $T=1.34175$ MeV: — — $^{233}\text{U}(n, F)$; — • — $^{233}\text{U}(n, F)$ [17]; — — — $^{235}\text{U}(n, F)$; Δ — $^{235}\text{U}(n, F)$ [11]; \circ — $^{235}\text{U}(n, F)$ [18], $E_n = 1$ — 2 MeV; ∇ — $^{235}\text{U}(n, F)$ [29]; \square — $^{235}\text{U}(n, F)$ [30]; \circ — $^{235}\text{U}(n, F)$ [31].

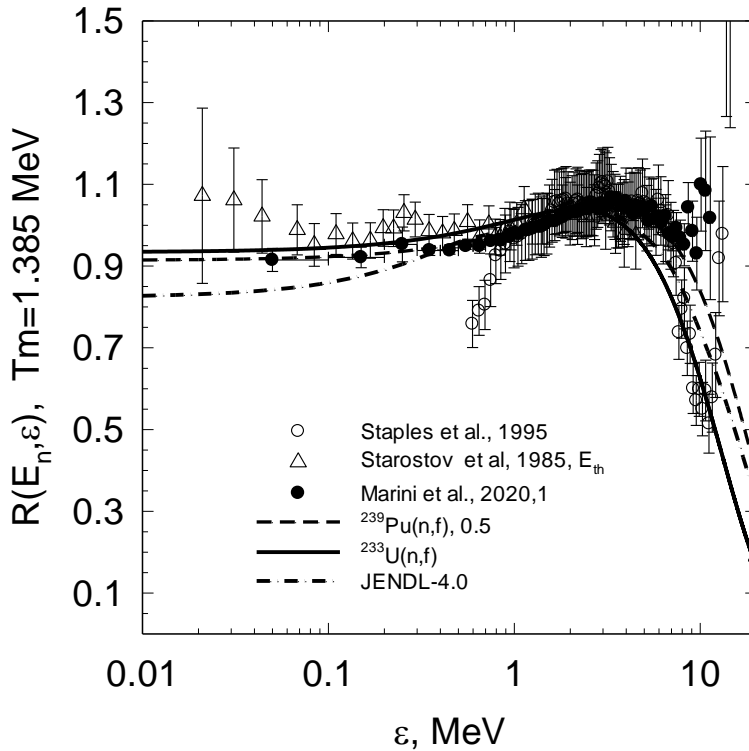


Fig.6. Prompt fission neutron spectra at $E_n = 0.5$ MeV relative to Maxwellian-type distribution with $T = 1.34175$ MeV: — — $^{233}\text{U}(n, F)$; — • — $^{233}\text{U}(n, F)$ [17]; — — — $^{235}\text{U}(n, F)$; Δ — $^{235}\text{U}(n, F)$ [11]; \circ — $^{235}\text{U}(n, F)$ [18], $E_n = 1$ — 2 MeV; ∇ — $^{235}\text{U}(n, F)$ [29]; \square — $^{235}\text{U}(n, F)$ [30]; \circ — $^{235}\text{U}(n, F)$ [31]; Δ — $^{239}\text{Pu}(n, F)$ [6]; \bullet — $^{239}\text{Pu}(n, F)$ [15], $E_n = 1$ — 2 MeV; \circ — $^{239}\text{Pu}(n, F)$ [31].

Here T_{xj} – “temperatures” of light and heavy fragments ($j=l, h$) of $(A+2-x)$ -th nuclide fissioning after pre-fission neutron emission. In equations (3–5) energy of center-of-mass

system per nucleon is $E_{vij}^0 = \frac{A_{hx}}{A_{lx}A_x} \cdot \alpha \cdot E_{fx}^{pre}$. It is assumed that light and heavy fragments emit

the same number of neutrons is a simplification, however it is well-known that calculated observed PFNS are not much sensitive to the inclusion of $\nu_p(E_n, A_{l(h)})$ instead of $\nu_p(E_n)$ by [25].

The ratio of “temperatures” of light and heavy fragments T_{xl}/T_{xh} , $r=1.1215$ is a semi-empirical parameter which is independent on (Z, N) values of fissioning nuclide, its value fits PFNS of $^{233}\text{U}(n_{th}, F)$, $^{235}\text{U}(n_{th}, F)$ and $^{239}\text{Pu}(n_{th}, F)$, the value of k_{ij} depends on the level density parameter.

Value of the parameter α — is the ratio of the fragment kinetic energy TKE at the moment of the neutron emission to the TKE at full acceleration of the fragments, $\alpha=0.860$ for ^{234}U , ^{233}U , ^{232}U и ^{231}U fissioning nuclides.

Average energy of PFNS $\langle E \rangle$ in laboratory system l.s. is $\langle E \rangle = \langle \varepsilon \rangle + E_v$, here $\langle \varepsilon \rangle$ — average energy of PFN in c.m., while E_v —Watt distribution parameter, i.e. energy of c.m. system in l.s. per nucleon. Usual assumption is that majority of neutrons is evaporated from fully accelerated fragment, however, it might be assumed that just upon scission some neutrons might be evaporated as well. The kinetic energy of fission fragments E_v is defined with the value of parameter “ α_1 ”, in that way PFNS of $^{235}\text{U}(n, F)$, $^{238}\text{U}(n, F)$, $^{239}\text{Pu}(n, F)$ and $^{232}\text{Th}(n, F)$ were reproduced [10, 26–32]. Calculated PFNS of $^{239}\text{Pu}(n, F)$ and $^{235}\text{U}(n, F)$ [10] at $E_n > E_{n2nf}$, were confirmed by measured data [11–13].

Various pairs of fission fragments with specific values of E_{fx}^{pre} contribute to the observed PFNS, the α_l parameter would be used as $E_{vij} = \alpha_l E_{vij}^0$, to compensate the major approximation of pair of average fragments, average fission energy and average value of TKE, note that $\alpha_l=1$ if $E_n < 6$ MeV, while $\alpha_l=0.8$ if $E_n > 12$ MeV, and α_l varies linearly in between.

TKE values of E_F^{pre} , kinetic energy before neutron emission from the fragments are superposition of TKE nuclides contributing to the observed fission cross section:

$$E_F^{pre}(E_n) = \sum_{x=0} E_{fx}^{pre}(E_{nx}) \cdot \sigma_{n,xf} / \sigma_{n,F} . \quad (6)$$

The excitation energy E_{nx} of $A, \dots, A+1-x$ nuclides, formed after emission of $(n, xnf)^{1 \dots x}$ pre-fission neutrons, depends on their average energies $\langle E_{n,xf}^k \rangle$:

$$E_{nx} = E_r - E_{fx}^{pre} + E_n + B_n - \sum_{x=0, 1 \leq k \leq x} (\langle E_{n,xf}^k \rangle + B_{nx}) . \quad (7)$$

Kinetic energy E_F^{post} of fission products, which emerge after emission of pre-fission neutrons, but before β^- -decay, equals

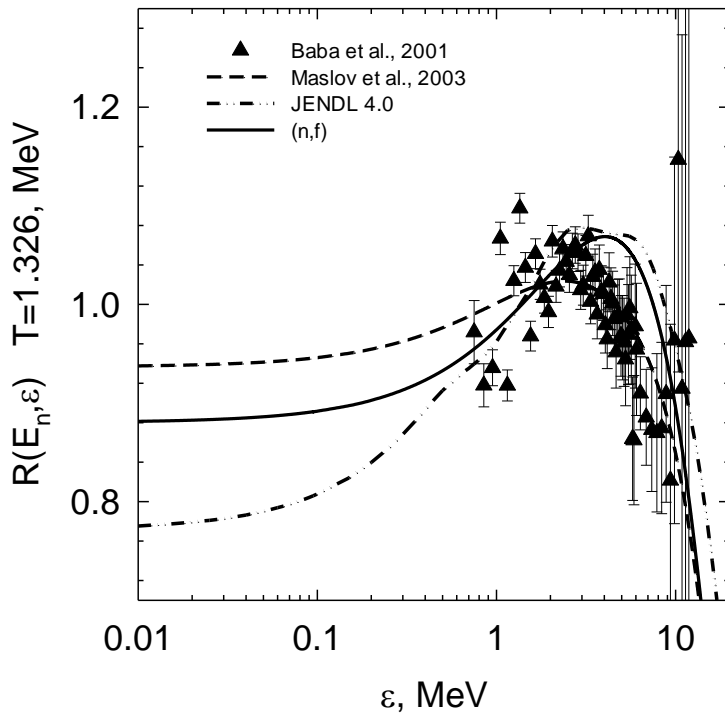


Fig.7. Prompt fission neutron spectra at $E_n = 0.5$ MeV relative to Maxwellian-type distribution with $T=1.326$ MeV: — $^{233}\text{U}(n, F)$; —•— $^{233}\text{U}(n, F)$ [17]; — — $^{235}\text{U}(n, F)$; Δ — $^{235}\text{U}(n, F)$ [11]; \circ — $^{235}\text{U}(n, F)$ [18], $E_n = 1-2$ MeV; ∇ — $^{235}\text{U}(n, F)$ [29]; \square — $^{235}\text{U}(n, F)$ [30]; \circ — $^{235}\text{U}(n, F)$ [31]; Δ — $^{239}\text{Pu}(n, F)$ [6]; \bullet — $^{239}\text{Pu}(n, F)$ [15], $E_n = 1-2$ MeV; \circ — $^{239}\text{Pu}(n, F)$ [31]; — — — — [4, 5]; \blacktriangle — [7].

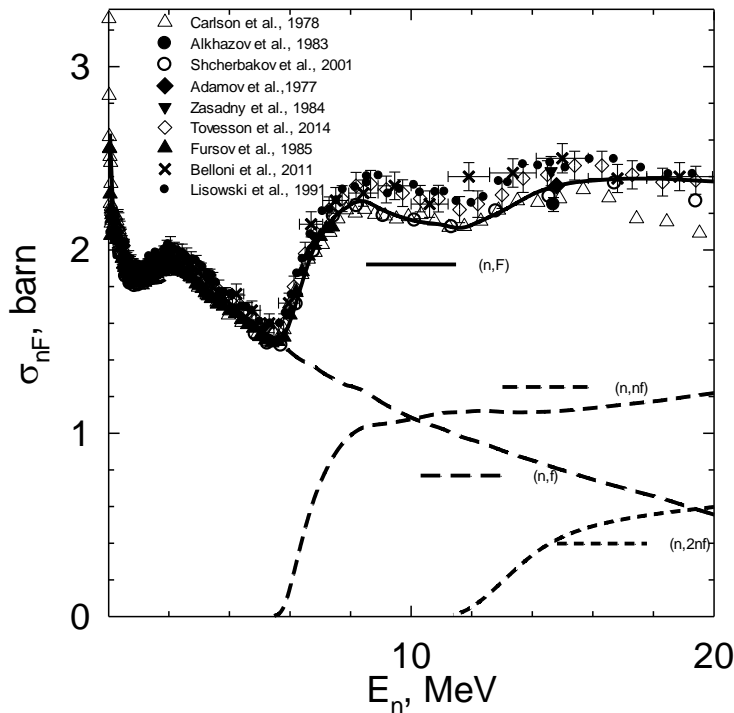


Fig.8. Partial components of $^{233}\text{U}(n, F)$; \blacktriangle — [52]; \blacklozenge — [53]; \bullet — [54]; \circ — [55], Δ — [56]; \blacktriangledown — [57]; \diamond — [58]; \bullet — [59]; \times — [60]

$$E_F^{post} \approx E_F^{pre} \left(1 - \nu_{post} / (A + 1 - \nu_{pre}) \right). \quad (8)$$

Similar equation for E_F^{post} was employed was used in [33] at $E_n < E_{n,f}$. At $E_n = 20$ MeV pre-fission neutron contribution ν_{pre} amounts to $\sim 0.15\nu_p$. Average prompt fission neutron number $\nu_p(E_n)$ is calculated as

$$\nu_p(E_n) = \nu_{post} + \nu_{pre} = \sum_{x=1} \nu_{px}(E_{nx}) + \sum_{x=1} (x-1) \cdot \beta_x(E_n). \quad (9)$$

Weak variations of TKE values, both E_F^{pre} and E_F^{post} , in the vicinity of $^{233}\text{U}(n,xf)$ reaction thresholds, as revealed in [34], are due to the decrease of excitation energy of $(A+I-x)$ fissioning nuclides after emission of x pre-fission neutron [35]. Local maxima in kinetic energy TKE at $E_n > E_{n,f}$, before and after pre-fission neutron emission for Z -even, N -odd target nuclide were observed in $^{235}\text{U}(n,F)$ [36–38] and $^{239}\text{Pu}(n,F)$ [39–41], in the vicinity of (n,nf) and $(n,2nf)$ reaction thresholds.

The contribution of $^{233}\text{U}(n,nf)$ reaction to the observed fission cross section $^{233}\text{U}(n,F)$ is governed by the fissility (fission probability) of ^{233}U nuclide, which is well-investigated in $^{232}\text{U}(n,F)$ reaction. Since $B_n(^{233}\text{U}) \sim B_f(^{233}\text{U})$ [42], fission probability is rather high, first-chance fission cross section $\sigma_{n,f}^{233}\text{U}(n,f)$ decreases with increase of E_n (see Fig. 8), the fission chances distribution for $^{233}\text{U}(n,F)$ is much different from those of other N -odd target nuclides $^{235,237}\text{U}$. In case of N -even target nuclides $^{234-238}\text{U}$ such sharp differences of first-chance fission cross sections $\sigma_{n,f}$ are not observed.

Fission cross section of $^{233}\text{U}(n,F)$ in the energy range $E_n \sim 0.01$ –20 MeV is thoroughly investigated [43–53], however, two data sets of [43–49] and [50–53] are systematically different. Absolute measurements of $\sigma_{n,F}$ [45] and [46, 47] at $E_n \sim 1.93$ MeV and $E_n \sim 14.7$, respectively, support data the measured relative to $\sigma_{n,F}^{235}\text{U}(n,F)$ [43, 44, 48, 49]. Time-of-flight measurements [51–53] are poorly described as regards the absolute values of fission cross sections of $^{233}\text{U}(n,F)$ and $^{235}\text{U}(n,F)$, they deviate from the first group data [43–49] by $\sim 7\%$. Present calculated fission cross section of $^{233}\text{U}(n,F)$, as those of [4, 5], are consistent with data of [43–49] (see Fig. 8). Hauser-Feshbach modelling of $\sigma_{n,F}$ at $E_n < 0.6$ MeV is sensitive to the positions of discrete transition states at the higher outer saddle point of ^{234}U double-humped fission barrier. When $E_n > 0.6$ MeV $\sigma_{n,F}$ is governed by the density of few-quasi-particle states of ^{234}U and ^{233}U at saddle and equilibrium deformations, respectively. When $E_n > E_{n,f}$, the $\sigma_{n,F}$ is governed by the density of excited states of ^{234}U , ^{233}U , ^{232}U and ^{231}U nuclides, which emerge during sequential pre-fission neutron emission, the first pre-fission neutron might be emitted in a pre-equilibrium/semi-direct fashion. Similar analysis was accomplished in case of $^{235}\text{U}(n,F)$ [26] and $^{237}\text{U}(n,F)$ [54] reactions.

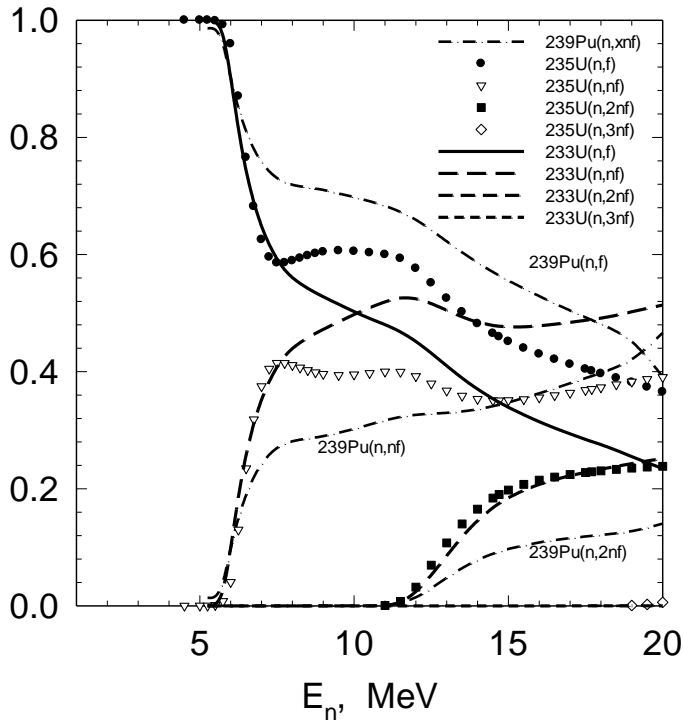


Fig.9. Ratios of partial components (n, xnf) to the observed fission cross section (n, F) ; — $^{233}\text{U}(n, F)$; — • — $^{235}\text{U}(n, F)$; ••• — $^{239}\text{Pu}(n, F)$.

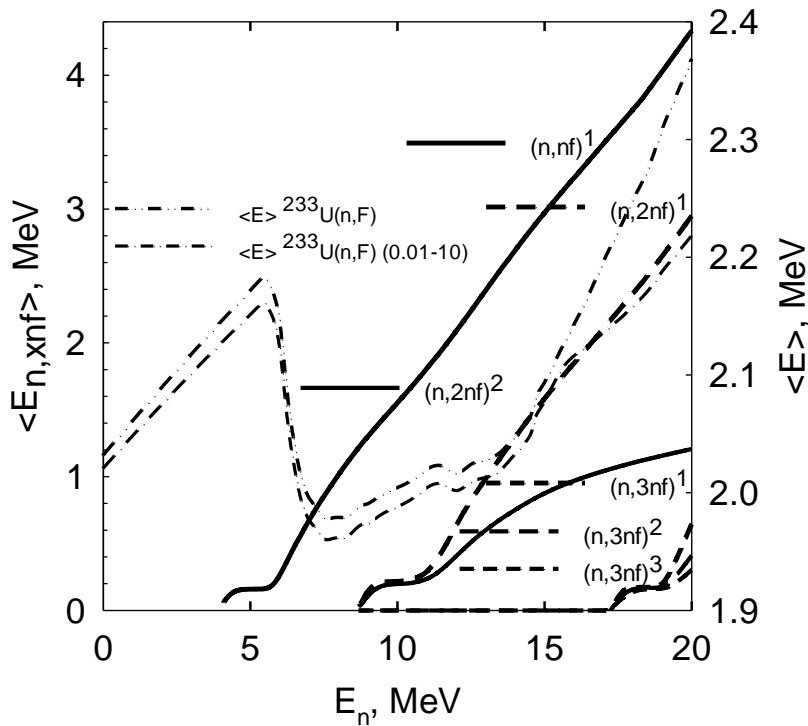


Fig.10. Average energy of exclusive pre-fission neutron spectra $^{233}\text{U}(n, xnf)$: —••, •••, —••• — $^{233}\text{U}(n, nf)^1$, $^{233}\text{U}(n, 2nf)^1$ и $^{233}\text{U}(n, 3nf)^1$, respectively; —•••, —••• — $^{233}\text{U}(n, 2nf)^2$, $^{233}\text{U}(n, 3nf)^2$, respectively; —••• — $^{233}\text{U}(n, 3nf)^3$; and PFNS $\langle E \rangle$: —••• — $\epsilon = 0-20$ MeV; —••• — $\epsilon = 0.01-10$ MeV.

Pre-fission $(n, xnf)^1$ neutron spectra

First pre-fission $^{233}\text{U}(n, nf)^1$ neutron spectra is calculated

$$\frac{d\sigma_{nnf}^1}{d\varepsilon} = \frac{d\sigma_{nnx}^1(\varepsilon)}{d\varepsilon} \frac{\Gamma_f^A(E_n - \varepsilon)}{\Gamma^A(E_n - \varepsilon)}, \quad (10)$$

here and if not stated otherwise upper index signifies the first sequential neutron in a specific reaction. Figure 9 shows $\beta_x(E_n) = \sigma_{n, xnf} / \sigma_{n, F}$ —partial contributions of observed fission cross sections $^{233, 235}\text{U}(n, F)$. Competition of fission and neutron emission for U(Pu) nuclides defines exclusive neutron spectra $(n, xnf)^{1\dots x}$ and $(n, xn)^{1\dots x}$. First neutron spectra of $^{233, 235}\text{U}(n, nx)^1$ reactions — $\frac{d\sigma_{nnx}^1(\varepsilon)}{d\varepsilon}$ are normalized by consistent description of $^{232}\text{U}(n, F)$, $^{233}\text{U}(n, F)$, $^{235}\text{U}(n, F)$, $^{234}\text{U}(n, F)$ and $^{235}\text{U}(n, 2n)$ reaction cross sections. Important feedback comes from neutron emission spectra of $^{235}\text{U}+n$ [23]. Average energies $\langle E_{n, xnf}^k \rangle$ of exclusive neutron spectra $^{233}\text{U}(n, xnf)^{1\dots x}$ are shown on Fig. 10. Average energies relevant for the (n, nf) and $(n, 2nf)^1$ reactions are rather hard, while exclusive neutron spectra of $(n, 2nf)^2$ and $(n, 3nf)^{1, 2, 3}$ reactions are of evaporation shape.

The shape of observed PFNS at $E_n \sim 6\text{--}11$ MeV correlates with fission probability of nuclei which emerge in (n, xnf) reactions, and $(n, xn\gamma)$ reaction cross sections. Exclusive neutron spectra (n, nf) , $(n, n\gamma)$ and $(n, 2n)^{1, 2}$ define the variation of relative amplitudes of (n, nf) reactions as dependent on the properties of $A+1$ and A nuclides with increase of incident neutron energy E_n . Figures 11–15 show calculated and measured PFNS of $^{233}\text{U}(n, F)$ in the vicinity of $^{233}\text{U}(n, nf)$ and $^{235}\text{U}(n, nf)$ reaction thresholds. The partial components of observed PFNS shown on Figs. 11–15 are the ratios to the maxwellian spectra with temperature around $2/3 \langle E \rangle$. Subtracting calculated PFNS of $^{235}\text{U}(n, f)$ reaction from the observed PFNS one gets semi-experimental estimate of the $^{235}\text{U}(n, nf)$ reaction contribution to the PFNS, as shown at the bottom of figures. Figures 11–15 show partial contributions to the PFNS of $^{233, 235}\text{U}(n, f)$ and $^{233, 235}\text{U}(n, nf)$. Variations of PFNS shape with increase of E_n for $^{233}\text{U}(n, nf)$ and $^{235}\text{U}(n, nf)$, are similar, however, the influence of $\beta_x(E_n)$ differences and relative shifts of (n, nf) and $(n, 2n)$ reactions thresholds is quite evident. Figures 11–15 demonstrate also pre-fission neutron contributions $\beta_2(E_n) v_p^{-1}(E_n) d\sigma_{nnf}^1 / d\varepsilon$ of $^{233}\text{U}(n, nf)^1$ and $^{235}\text{U}(n, nf)^1$. Pre-fission neutrons influence observed PFNS both at $\varepsilon < \langle E \rangle$ and at $\varepsilon > \langle E \rangle$. Contribution of $(n, nf)^1$ neutrons of $^{233}\text{U}(n, F)$ reaction at $E_n \sim 6$ MeV and $E_n \sim 6.5$ MeV are higher than in case of $^{235}\text{U}(n, F)$ reaction. The observed PFNS of $^{233}\text{U}(n, F)$ and $^{235}\text{U}(n, F)$ are similar, since the increase of contribution of $^{233}\text{U}(n, nf)$ reaction is accompanied by extraordinary decrease of $^{233}\text{U}(n, f)$ reaction contribution.

When the (n, nf) reaction competes with the $(n, n\gamma)$ reaction only, the pre-fission neutron shapes depend on the fissilities of A and $A+1$ nuclides only weakly. After the $(n, 2n)$ reaction channel opens, the (n, nf) pre-fission neutron shape turns to be rather sensitive to the influence

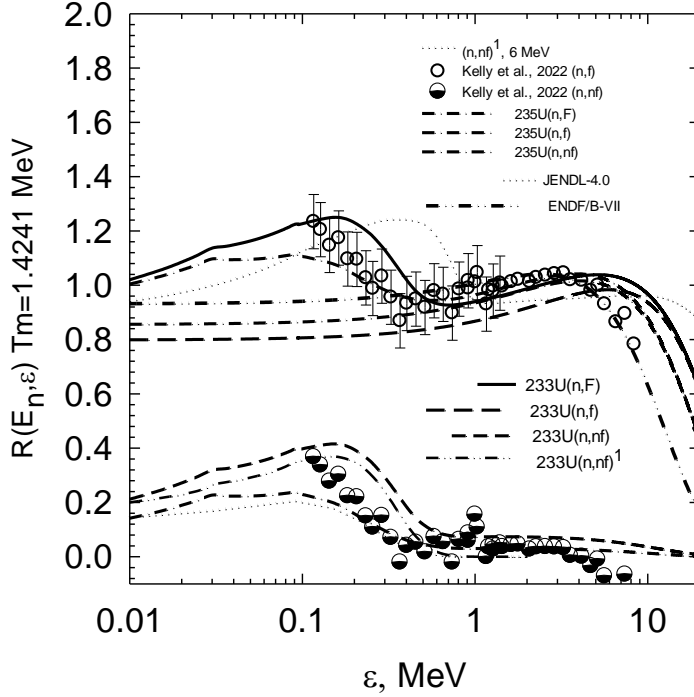


Fig.11. Ratios of partial (n,xf) components of PFNS at $E_n = 6,0$ MeV of $^{233}\text{U}(n, F)$ relative to Maxwellian-type distribution with $T = 1.4241$ MeV: — $^{233}\text{U}(n,F)$; - - - $^{233}\text{U}(n,f)$; - · - $^{233}\text{U}(n,nf)$; ··· $^{233}\text{U}(n,nf)^1$; - · - $^{235}\text{U}(n,F)$, $^{235}\text{U}(n,f)$, $^{235}\text{U}(n,nf)$; ○ — $^{235}\text{U}(n,F)$ [13]; Δ — $^{235}\text{U}(n,nf)$ [13]; ··· —

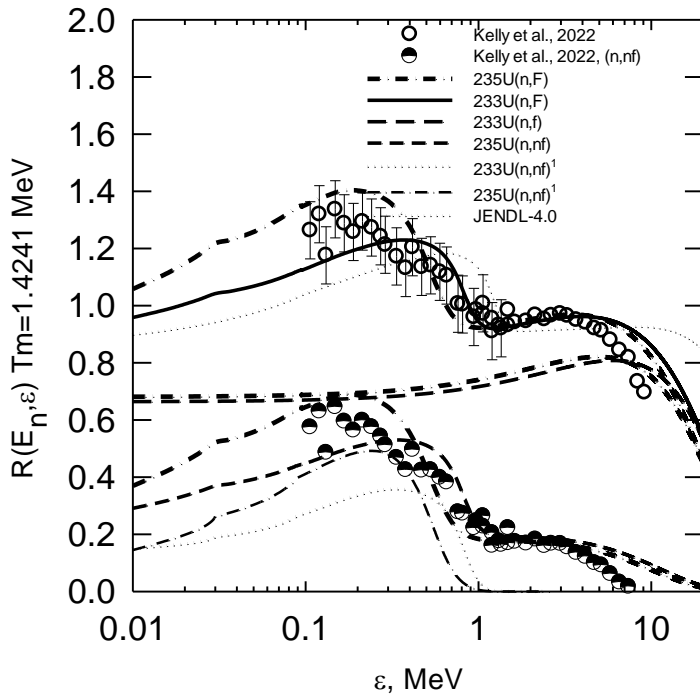


Fig.12. Ratios of partial (n,xf) components of PFNS at $E_n = 6,5$ MeV of $^{233}\text{U}(n, F)$ relative to Maxwellian-type distribution with $T = 1.4241$ MeV: — $^{233}\text{U}(n,F)$; - - - $^{233}\text{U}(n,f)$; - · - $^{233}\text{U}(n,nf)$; ··· $^{233}\text{U}(n,nf)^1$; - · - $^{235}\text{U}(n,F)$, $^{235}\text{U}(n,f)$, $^{235}\text{U}(n,nf)$; ○ — $^{235}\text{U}(n,F)$ [13]; Δ — $^{235}\text{U}(n,nf)$ [13]; ··· — $^{235}\text{U}(n,nf)^1$; — · — ENDF/B-VII [16]; — · — JENDL-4.0 [17].

of exclusive $(n,2n)^1$ and $(n,2n)^2$ neutron spectra. For the reaction $^{233}\text{U}(n,nf)$ at $E_n > 6$ MeV the competition of $^{233}\text{U}(n,2n)$, since the threshold of $(n,2n)$ reaction $E_{n2n} \sim 5.7$ MeV, is important. At $E_n \sim 7$ MeV when $\varepsilon \sim 0.8$ MeV, close to the peak of the PFNS, $\tilde{S}_{233}(\varepsilon, E_n) \sim \tilde{S}_{234}(\varepsilon, E_n)$, while for $^{235}\text{U}(n,F)$, $\tilde{S}_{235}(\varepsilon, E_n) \sim 1.1 \tilde{S}_{236}(\varepsilon, E_n)$ (Fig. 13). Another peculiarity is that fission fragments of ^{234}U are relatively more “heated” than those of ^{236}U .

The influence of $^{233}\text{U}(n,nf)^1$ exclusive pre-fission neutrons on the observed $\langle E \rangle$ of $^{233}\text{U}(n,F)$ PFNS is quite strong, at $E_n \sim 6$ MeV relative amplitudes $\beta_2(E_n) \nu_p^{-1}(E_n) d\sigma_{nf}^1 / d\varepsilon$ are systematically higher than those of $^{235}\text{U}(n,F)$ reaction. The highest relative amplitude is observed at $E_n \sim 6$ MeV for $^{233}\text{U}(n,F)$ and at $E_n \sim 6.5$ MeV in case of $^{235}\text{U}(n,F)$ reaction (see Fig. 11 and Fig. 12). In left lower corner of the Figure 13 the relative amplitudes $\beta_2(E_n) \nu_p^{-1}(E_n) d\sigma_{nf}^1 / d\varepsilon$ of exclusive pre-fission neutron spectra $^{233}\text{U}(n,nf)^1$ and $^{235}\text{U}(n,nf)^1$ at $E_n \sim 6.0; 6.5; 7.0$ MeV are shown, systematic differences are evident.

With increase of E_n the contributions of $\tilde{S}_A(\varepsilon, E_n)$ and $\tilde{S}_{A+1}(\varepsilon, E_n)$ vary quite appreciably. With increase of average energies of exclusive pre-fission neutron spectra $\langle E_{n,nf}^k \rangle$ the contribution of neutrons emitted from the second chance fission fragments to the $\tilde{S}_A(\varepsilon, E_n)$, decreases, as ε increases, much faster than that of $\tilde{S}_{A+1}(\varepsilon, E_n)$. Comparing the contributions of $\tilde{S}_{234}(\varepsilon, E_n)$ and $\tilde{S}_{233}(\varepsilon, E_n)$ of $^{233}\text{U}(n,F)$ at $E_n \sim 8.5$ MeV one may conclude that fission fragments of ^{234}U are more “heated”, than fission fragments of ^{233}U (see Fig. 14). The most expressive snap-shot is the difference of partial contributions of $^{233}\text{U}(n,F)$ and $^{235}\text{U}(n,F)$ PFNS at $E_n \sim 10.5$ MeV (see Fig. 15). Figure 15 demonstrates also ENDF/B-VII evaluation of $^{233}\text{U}(n,F)$ PFNS. It seems that in ENDF/B-VII evaluation they almost waived off pre-fission neutrons contribution. In case of JENDL-4.0 the contribution of pre-fission neutrons to the observed PFNS is too high.

Exclusive pre-fission neutron spectrum contains pre-equilibrium/semi-direct component, the hard energy part of exclusive pre-fission neutron spectrum of $(n,nf)^1$ reaction is defined by the fission probability of target nuclide A, ^{233}U (^{235}U in case of $^{235}\text{U}(n,F)$). There is no experimental data on $^{233}\text{U}+n$ to estimate reliably the hard energy part of $(n,nf)^1$ reaction neutron spectrum. In case of $^{238}\text{U}+n$ interaction the neutron emission spectra exhibit strong angular anisotropy, the residual nuclides ^{238}U remain at excitations of $U=1\sim 6$ MeV [55]. Direct excitation of ^{238}U ground state band levels $J^\pi = 0^+, 2^+, 4^+, 6^+, 8^+$ was accomplished within rigid rotator model, while that of β -bands of $K^\pi = 0^+$ and γ -bands of $K^\pi = 2^+$, octupole band of $K^\pi = 0^-$ was accomplished within soft deformable rotator [56]. The net effect of these procedures is the adequate approximation of angular distributions of $(n,nX)^1$ first neutron inelastic scattering in continuum

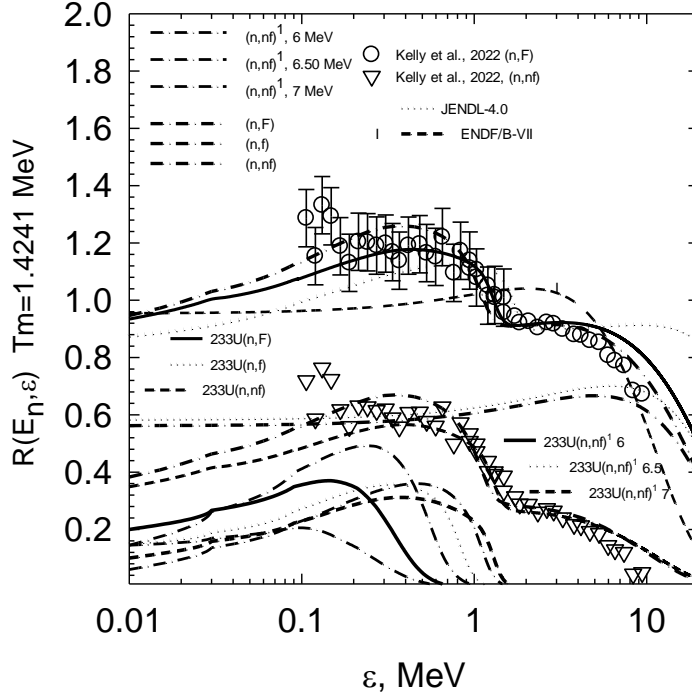


Fig.13. Ratios of partial (n,xf) components of PFNS at $E_n = 7,0$ MeV of $^{233}\text{U}(n, F)$ relative to Maxwellian-type distribution with $T = 1.4241$ MeV: — — — — exclusive pre-fission neutron spectra $^{233}\text{U}(n,xf)^1$, 6 MeV; ••• — 6.5 MeV; — — — — 7 MeV; — • — — $^{235}\text{U}(n,F)$, $^{235}\text{U}(n,f)$, $^{235}\text{U}(n,nf)$; — — — — exclusive pre-fission neutron spectra of $^{235}\text{U}(n,xf)^1$, 6 MeV; ••• — 6.5 MeV; — — — — 7 MeV; ∇ — $^{235}\text{U}(n,nf)$ [18].

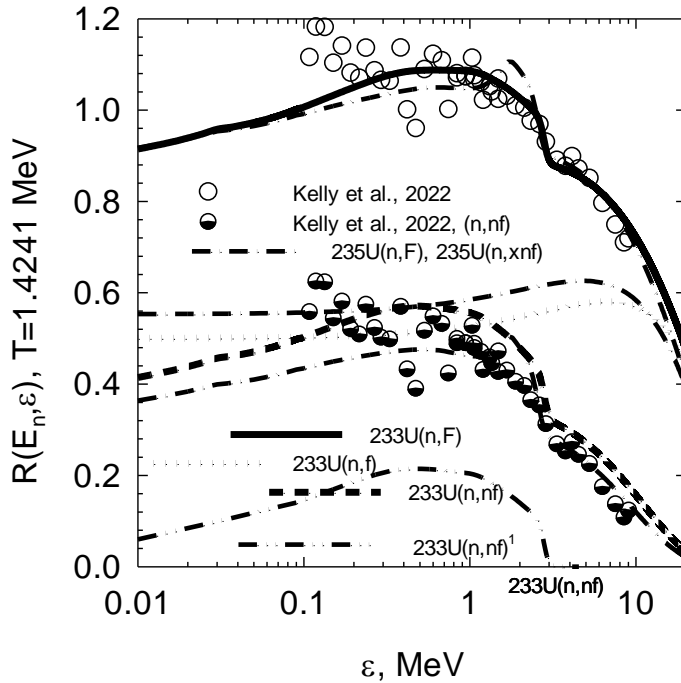


Fig.14. Ratios of partial (n,xf) components of PFNS at $E_n = 8.5$ MeV of $^{233}\text{U}(n, F)$ relative to Maxwellian-type distribution with $T = 1.4241$ MeV: — — — — exclusive pre-fission neutron spectra $^{233}\text{U}(n,xf)^1$, 6 MeV; ••• — 6.5 MeV; — — — — 7 MeV; — • — — $^{235}\text{U}(n,F)$, $^{235}\text{U}(n,f)$, $^{235}\text{U}(n,nf)$; — — — — exclusive pre-fission neutron spectra of $^{235}\text{U}(n,xf)^1$, 6 MeV; ••• — 6.5 MeV; — — — — 7 MeV; ∇ — $^{235}\text{U}(n,nf)$ [18].

$$d\sigma_{nmx}^1/d\varepsilon \approx d\tilde{\sigma}_{nmx}^1/d\varepsilon + \sqrt{\frac{\varepsilon}{E_n}} \frac{\langle \omega(\theta) \rangle_\theta}{E_n - \varepsilon}, \quad (11)$$

here $d\tilde{\sigma}_{nmx}^1/d\varepsilon$ corresponds to the compound emission, which is angle-independent with respect to the incident beam. The adequate approximation of angular distributions of $^{238}\text{U}(n,nX)^1$ first neutron inelastic scattering in continuum which corresponds to $U=1.16\sim 6$ MeV excitations for $E_n = 1.16$ MeV ~ 20 MeV [55] was obtained. The obtained approximation was employed in case of $^{235}\text{U}+n$ and $^{233}\text{U}+n$ interactions. The anisotropic part of first neutron spectrum relevant to excitations, comparable with ^{233}U fission barrier value, would be evidenced in $(n, xn f)$ spectra, however, it would be pronounced mostly in neutron spectra of $(n, n\gamma)^1$, $(n, 2nf)^1$ and $(n, 2n)^1$ reactions at $E_n > 12$ MeV and, consequently, in PFNS observed at various angles with respect to the incident beam [57].

First neutron spectra of $(n, 2nx)$, or equivalently, $(n, 2nx)^1$, depends on the first neutron spectra of $(n, nX)^1$ and the probability of neutron emission from the nuclide A as:

$$\frac{d\sigma_{n2nx}^1}{d\varepsilon} = \frac{d\sigma_{nmx}^1(\varepsilon)}{d\varepsilon} \frac{\Gamma_n^A(E_n - \varepsilon)}{\Gamma^A(E_n - \varepsilon)} \quad (12)$$

First neutron spectra of $^{233}\text{U}(n, 2nf)$, and $^{233}\text{U}(n, 2nf)^1$ are:

$$\frac{d\sigma_{n2nf}^1}{d\varepsilon} = \int_0^{E - B_n^{233}} \frac{d\sigma_{n2nx}^1(\varepsilon)}{d\varepsilon} \frac{\Gamma_f^{232}(E_n - B_n^A - \varepsilon - \varepsilon_1)}{\Gamma^{232}(E_n - B_n^A - \varepsilon - \varepsilon_1)} d\varepsilon_1 \quad (13)$$

Second neutron spectra of $(n, 2nx)$, $(n, 2nx)^2$, i.e. emission spectra from nuclide A , ^{233}U , calculated as

$$\frac{d\sigma_{n2nx}^2}{d\varepsilon} = \int_0^{E - B_n^A - \varepsilon} \frac{d\sigma_{n2nx}^1(\varepsilon)}{d\varepsilon} \frac{\Gamma_n^A(E_n - B_n^A - \varepsilon - \varepsilon_1)}{\Gamma^A(E_n - B_n^A - \varepsilon - \varepsilon_1)} d\varepsilon_1. \quad (14)$$

Spectra of second neutron of $(n, 2nf)$, or $(n, 2nf)^2$ are:

$$\frac{d\sigma_{n2nf}^2}{d\varepsilon} = \int_0^{E - B_n} \frac{d\sigma_{n2nx}^2(\varepsilon)}{d\varepsilon} \frac{\Gamma_f^{A-1}(E_n - B_n^A - \varepsilon_1 - \varepsilon_2)}{\Gamma^{A-1}(E_n - B_n^A - \varepsilon_1 - \varepsilon_2)} d\varepsilon_1 \quad (15)$$

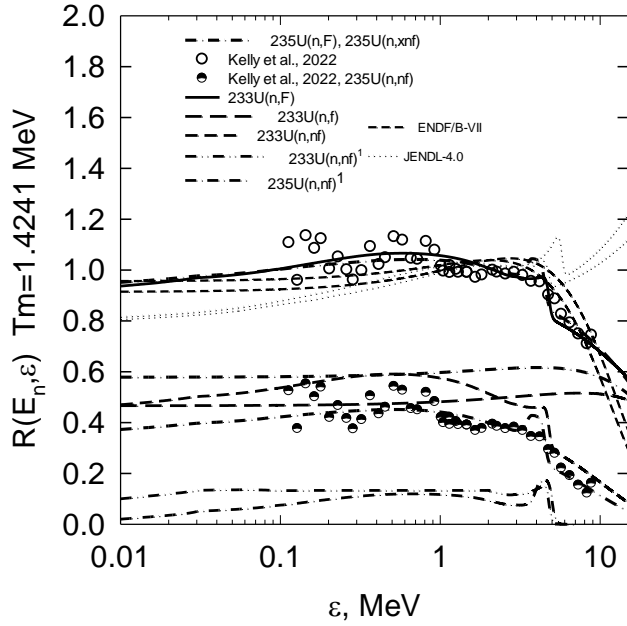


Fig.15. Ratios of partial (n, xnf) components of PFNS at $E_n = 10.5$ MeV of $^{233}\text{U}(n, F)$ relative to Maxwellian-type distribution with $T = 1.4241$ MeV: — — — — exclusive pre-fission neutron spectra $^{233}\text{U}(n, nf)^1$, 6 MeV; ••• — 6.5 MeV; — — — — 7 MeV; — • — — $^{235}\text{U}(n, F)$, $^{235}\text{U}(n, f)$, $^{235}\text{U}(n, nf)$; — — — — exclusive pre-fission neutron spectra of $^{235}\text{U}(n, nf)^1$, 6 MeV; ••• — 6.5 MeV; — — — — 7 MeV; ▽ — $^{235}\text{U}(n, nf)$ [18]; — • • — JENDL-4.0, $E_n = 10, 11$ MeV [17]; — • — — — — ENDF/B-VII, $E_n = 10$ MeV и $E_n = 11$ MeV [16]

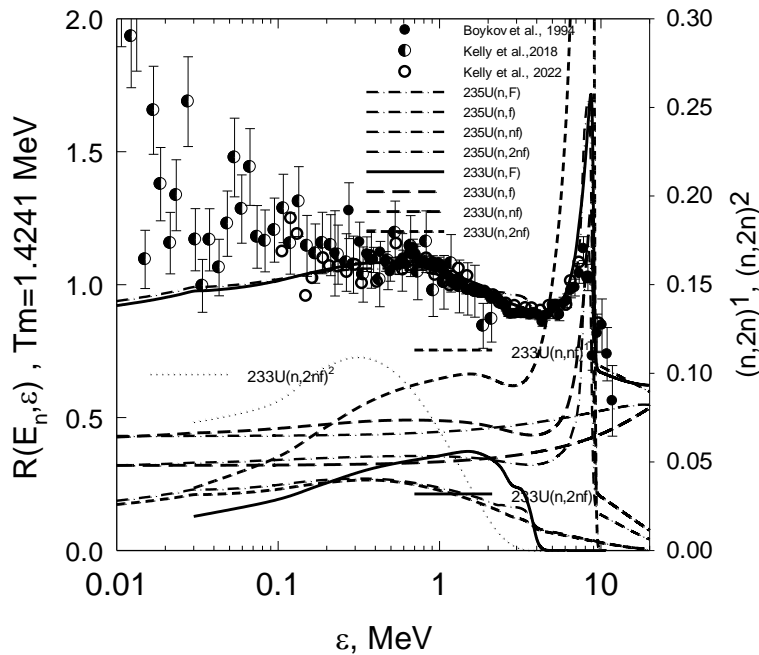


Fig.16. Ratios of partial components of PFNS $E_n = 14.7$ MeV of $^{233}\text{U}(n, F)$ relative to Maxwellian-type distribution with $T = 1.4241$ MeV: — — — — $^{233}\text{U}(n, F)$; — — — — $^{233}\text{U}(n, f)$; — — — — $^{233}\text{U}(n, nf)$; — — — — $^{233}\text{U}(n, 2nf)$; — • — — $^{235}\text{U}(n, F)$, $^{235}\text{U}(n, f)$, $^{235}\text{U}(n, nf)$, $^{235}\text{U}(n, 2nf)$; — — — — $^{233}\text{U}(n, nf)^1$; — — — — $^{233}\text{U}(n, 2nf)^1$; ••• — $^{233}\text{U}(n, 2nf)^2$; — • — — — — ENDF/B-VII [11]; — • • — — JENDL-4.0, $E_n = 14, 16$ MeV [17]; ○, Δ — $^{235}\text{U}(n, F)$ [18]; ● — $^{235}\text{U}(n, F)$ [67]

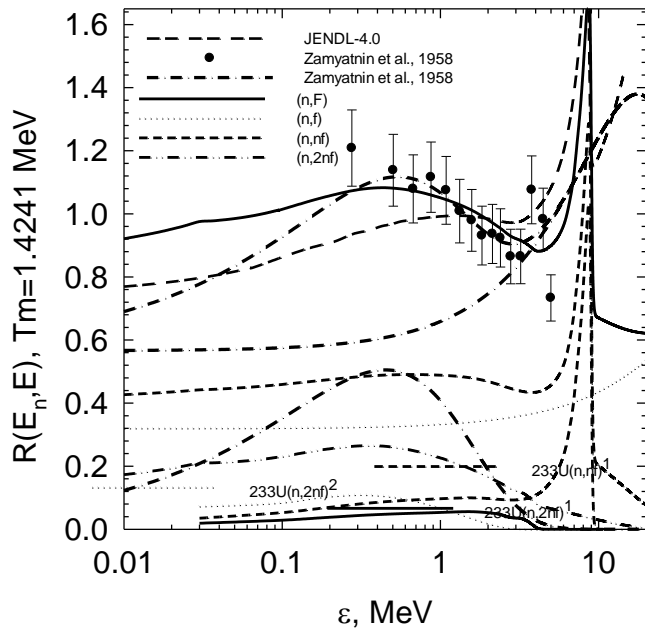


Fig.17. Ratios of partial components of PFNS $E_n \sim 14$ MeV of $^{233}\text{U}(n, F)$ relative to Maxwellian-type distribution with $T = 1.4241$ MeV: — $^{233}\text{U}(n, F)$; $\bullet\bullet\bullet$ — $^{233}\text{U}(n, f)$; $-\cdot-\cdot-$ $^{233}\text{U}(n, nf)$; $-\cdot\bullet-\cdot-$ $^{233}\text{U}(n, 2nf)$; — $^{233}\text{U}(n, F)$; $\bullet\bullet\bullet$ — $^{233}\text{U}(n, f)$; $-\cdot-\cdot-$ $^{233}\text{U}(n, xnf)$ [6]; \bullet — $^{233}\text{U}(n, F)$ [6]. $-\bullet-\bullet-$ — ENDF/B-VII [16]; $-\cdot\cdot-\cdot-$ — JENDL-4.0, $E_n = 14, 16$ MeV [17]

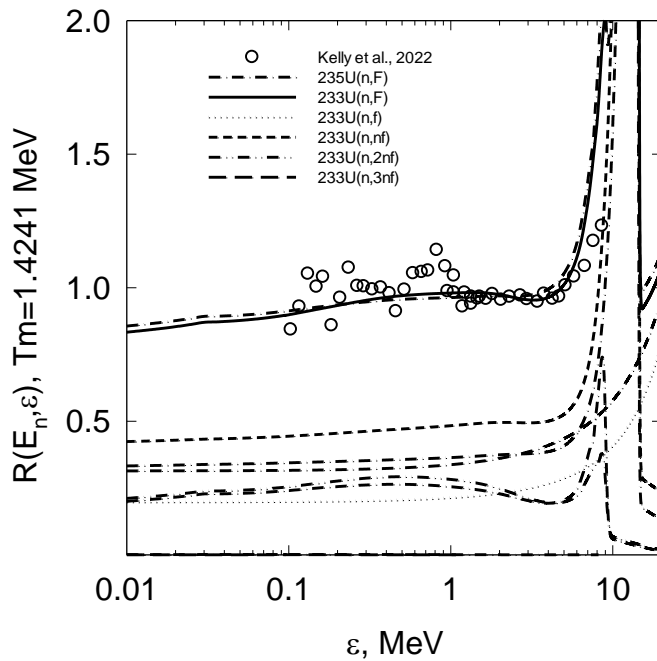


Fig.18. Ratios of partial components of PFNS $E_n \sim 20$ MeV of $^{233}\text{U}(n, F)$ relative to Maxwellian-type distribution with $T = 1.4241$ MeV: — $^{233}\text{U}(n, F)$; $\bullet\bullet\bullet$ — $^{233}\text{U}(n, f)$; $-\cdot-\cdot-$ $^{233}\text{U}(n, nf)$; $-\cdot\bullet-\cdot-$ $^{233}\text{U}(n, 2nf)$; — $^{233}\text{U}(n, F)$; $\bullet\bullet\bullet$ — $^{233}\text{U}(n, f)$; $-\cdot-\cdot-$ $^{233}\text{U}(n, xnf)$ [6]; \bullet — $^{233}\text{U}(n, F)$ [6]. $-\bullet-\bullet-$ — ENDF/B-VII [16]; $-\cdot\cdot-\cdot-$ — JENDL-4.0, $E_n = 14, 16$ MeV [17]

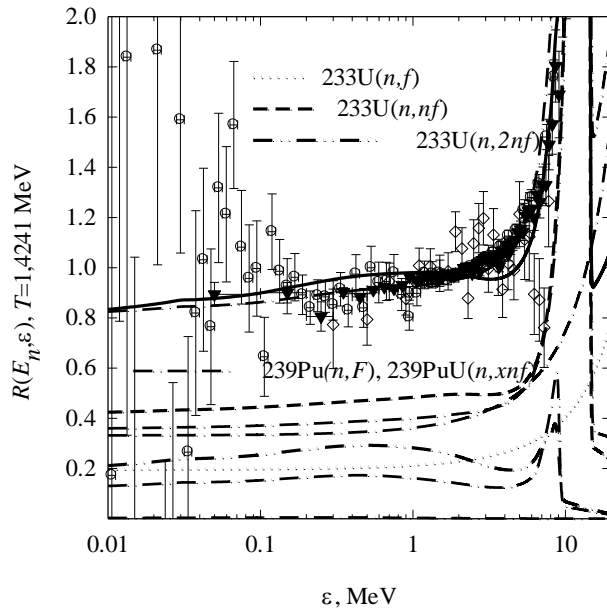


Fig.19. Ratios of partial components of PFNS $E_n \sim 20$ MeV of $^{233}\text{U}(n, F)$ relative to Maxwellian-type distribution with $T = 1.4241$ MeV: — $^{233}\text{U}(n, F)$; $\bullet\bullet\bullet$ — $^{233}\text{U}(n, f)$; $-\cdot-\cdot-$ — $^{233}\text{U}(n, nf)$; $-\cdot\cdot-\cdot-$ — $^{233}\text{U}(n, 2nf)$; $-\cdot-\cdot-$ — $^{233}\text{U}(n, F)$; $\bullet\bullet\bullet$ — $^{233}\text{U}(n, f)$; $-\cdot-\cdot-$ — $^{233}\text{U}(n, xnf)$ [6]; \bullet — $^{233}\text{U}(n, F)$ [6]. $-\cdot-\cdot-$ — ENDF/B-VII [16]; $-\cdot\cdot-\cdot-$ — JENDL-4.0, $E_n = 14, 16$ MeV [17]; $-\bullet-$ — $^{239}\text{Pu}(n, F)$, $^{39}\text{Pu}(n, f)$, $^{39}\text{Pu}(n, nf)$, $^{39}\text{Pu}(n, 2nf)$ и $^{39}\text{Pu}(n, 3nf)$; \circ — [19]; \blacktriangledown — [20]

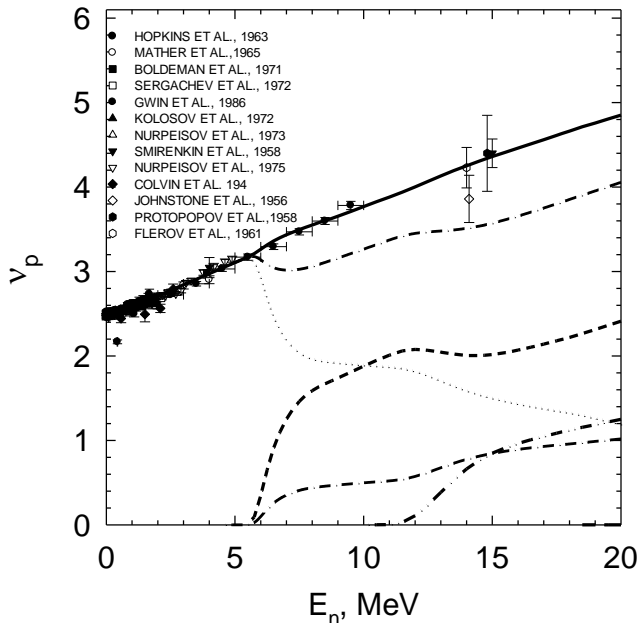


Fig.20. Average number of prompt fission neutrons of $^{233}\text{U}(n, F)$ and its partial components: — $^{233}\text{U}(n, F)$; $\bullet\bullet\bullet$ — $^{233}\text{U}(n, f)$; $-\cdot-\cdot-$ — $^{233}\text{U}(n, nf)$; $-\cdot\cdot-\cdot-$ — $^{233}\text{U}(n, 2nf)$; $-\bullet-$ — ν_{post} and ν_{pre} ; \bullet — [68]; \circ — [69]; \square — [70]; \blacksquare — [71]; Δ — [72]; ∇ — [73]; \square — [74]; \diamond — [75]; \blacklozenge — [76]; \blacktriangledown — [77]; \blacktriangle — [78]; \bullet — [79]; \diamond — [80]

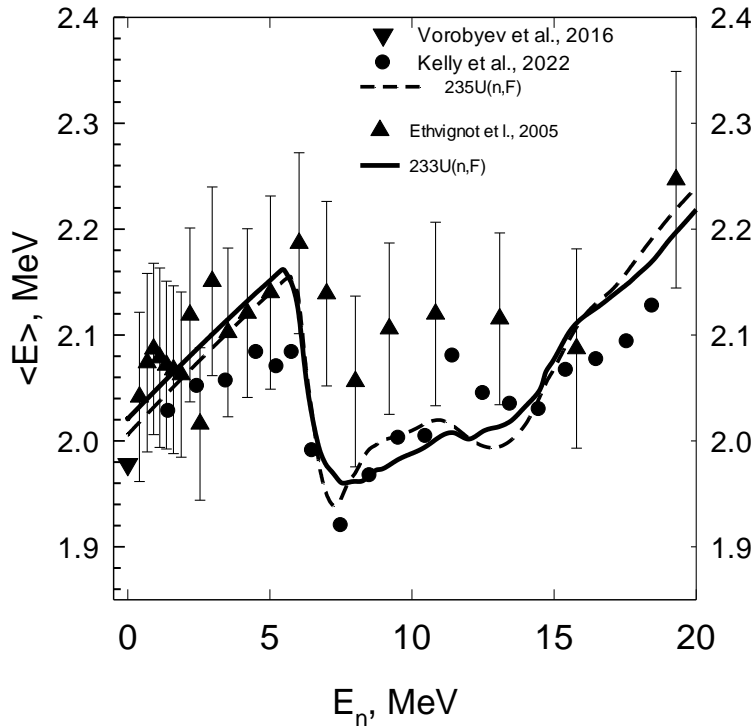


Fig.21. Average energy $\langle E \rangle$ of prompt fission neutrons of $^{233}\text{U}(n, F)$ ———, $^{235}\text{U}(n, F)$ — — —; ∇ — $^{233}\text{U}(n, F)$ [13]; \bullet — $^{235}\text{U}(n, F)$ [15]; \blacktriangle — $^{235}\text{U}(n, F)$ [81]

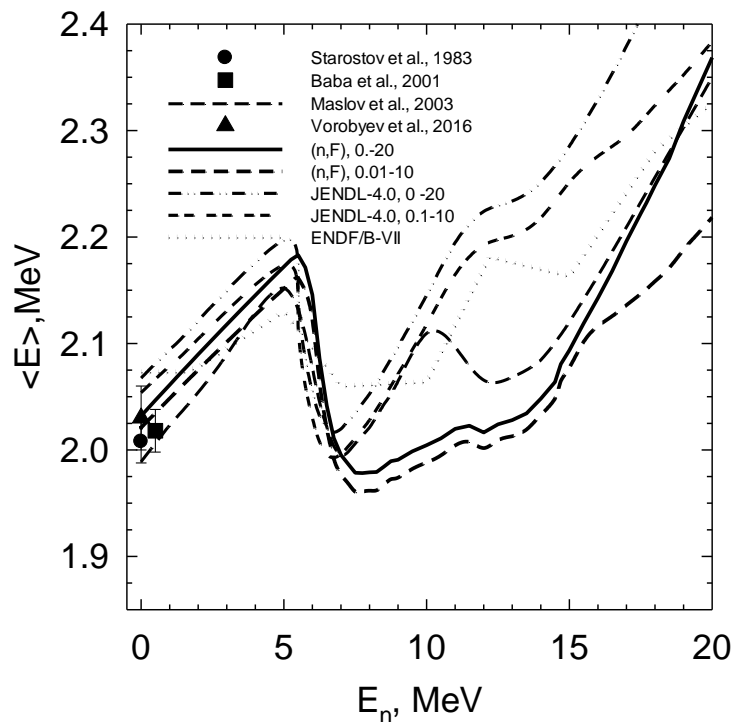


Fig.22. Average energy $\langle E \rangle$ of prompt fission neutrons of $^{233}\text{U}(n, F)$: ———, — — — — in the range $\epsilon \sim 0-20$ MeV and $\epsilon \sim 0.01-10$ MeV, respectively; — — — — [9,10]; \bullet — [11]; \blacksquare — [12]; \blacktriangle — [13]; —•—•— JENDL-4.0 [17] in the range $\epsilon \sim 0-20$ MeV and $\epsilon \sim 0.01-10$ MeV, respectively; —•—•— ENDF/B-VII [16].

Hard part of first neutron spectra $\frac{d\sigma_{n2nf}^1}{d\varepsilon}$ of $^{233}\text{U}(n,2nf)$ ($^{235}\text{U}(n,2nf)$) is defined by the fission probability of ^{233}U (^{235}U). Exclusive spectra of first and second neutrons of $^{233}\text{U}(n,2nf)$ ($^{235}\text{U}(n,2nf)$) are defined by fission probability of $^{233,232}\text{U}$ ($^{235,234}\text{U}$) nuclides.

Figure 16 shows partial contributions to the PFNS of $\tilde{S}_{A+1}(\varepsilon, E_n)$, $\tilde{S}_A(\varepsilon, E_n)$, $\tilde{S}_{A-1}(\varepsilon, E_n)$ and $\tilde{S}_{A-2}(\varepsilon, E_n)$ for $^{233}\text{U}(n,F)$ and $^{235}\text{U}(n,F)$ reactions [10] and measured PFNS data of $^{233}\text{U}(n,F)$ at $E_n \sim 14.7$ MeV [58]. Contribution of the (n,f) to the PFNS $^{233}\text{U}(n,F)$ is appreciably lower than in case of $^{235}\text{U}(n,F)$ reaction: $\tilde{S}_{234}(\varepsilon, E_n) \sim 0.6 \tilde{S}_{236}(\varepsilon, E_n)$. Contributions of (n,nf) reactions $\tilde{S}_{233}(\varepsilon, E_n)$ and $\tilde{S}_{235}(\varepsilon, E_n)$ represent a mirror case, in the vicinity of maximum contribution to the PFNS of $^{233}\text{U}(n,2nf)^{1,2}$ neutrons, $\tilde{S}_{233}(\varepsilon, E_n) \sim 1.5 \tilde{S}_{235}(\varepsilon, E_n)$. On Fig. 16 are shown partial contributions of $^{233}\text{U}(n,2nf)^1$ and $^{233}\text{U}(n,2nf)^2$, note that contributions of $^{233}\text{U}(n,2nf)$ and $^{235}\text{U}(n,2nf)$ reactions to the observed fission cross sections $^{233}\text{U}(n,F)$ and $^{235}\text{U}(n,F)$ almost coincide with each other, i.e. $\tilde{S}_{232}(\varepsilon, E_n) \sim \tilde{S}_{234}(\varepsilon, E_n)$. Exclusive spectra of pre-fission neutrons $\beta_2(E_n) \nu_p^{-1}(E_n) d\sigma_{nnf}^1 / d\varepsilon$, $\beta_3(E_n) \nu_p^{-1} \left[\frac{d\sigma_{n2nf}^1}{d\varepsilon} \right]$ and $\beta_3(E_n) \nu_p^{-1} \left[\frac{d\sigma_{n2nf}^2}{d\varepsilon} \right]$ of $^{233}\text{U}(n,F)$ have intricate dependence on the fission probability of the nuclides $^{234-x}\text{U}$, emerging in a successive emission of pre-fission neutrons in $^{233}\text{U}(n,xnf)$ reactions.

Notwithstanding the excessive simplification of Eq. (1), the data [1] and Eq. (1) are quite compatible the calculated $^{233}\text{U}(n,F)$ PFNS shape [4, 5], though in a narrow investigated energy range $0.3 < \varepsilon < 5$ MeV (see Fig. 17). In case of reaction $^{233}\text{U}(n,F)$ [1] average energy of evaporation neutron spectrum of Eq. (1) $\langle E_{n,nf} \rangle = 2T$ is quite consistent with average energy of exclusive pre-fission neutron spectra $d\sigma_{n2nf}^1 / d\varepsilon$ and $d\sigma_{n2nf}^2 / d\varepsilon$ of [4, 5, 10] and present calculations: $\langle E_{n2nf} \rangle = 0.5(\langle E_{n2nf}^1 \rangle + \langle E_{n2nf}^2 \rangle) \sim 1.2$ MeV. Exclusive first neutron spectrum of $^{233}\text{U}(n,2nf)^1$, $d\sigma_{n2nf}^1 / d\varepsilon$ at $E_n \sim 14$ MeV has a weak pre-equilibrium component. Due to its contribution average energy of $^{233}\text{U}(n,nf)^1$ reaction neutron amounts to $\langle E_{nnf} \rangle \sim 3$ MeV. Present pre-fission neutron spectrum is much different from the evaporation approximation of [1]. However, approximation of PFNS with Eq. (1) only qualitatively reproduces the contribution of “soft” pre-fission neutrons, net contribution of pre-fission neutrons with $\varepsilon < 1$ MeV and neutrons, evaporated from fission fragments of $^{233}\text{U}(n,f)$, $^{233}\text{U}(n,nf)$ and $^{233}\text{U}(n,2nf)$ reactions, and shape of prompt fission neutrons with energies $5 < \varepsilon < 20$ MeV, evaporated from fission fragments. Evaluation of ENDF/B–VII [14] – is an evaporation spectrum with variable average energy $\langle E \rangle$ and arbitrary shape of PFNS, in the next version of ENDF/B–VIII [16] it was abandoned being replaced by JENDL–4.0 evaluation [17].

New measurements of $^{235}\text{U}(n,F)$ and $^{239}\text{Pu}(n,F)$ PFNS [11–13] probe incident neutron energy range of $E_n \sim 1.5$ –20 MeV and prompt fission neutron energy range $\varepsilon \sim 0.01$ –10 MeV. The PFNS measured data supported the predictions of $^{235}\text{U}(n,F)$ PFNS [13, 26, 28, 30] and

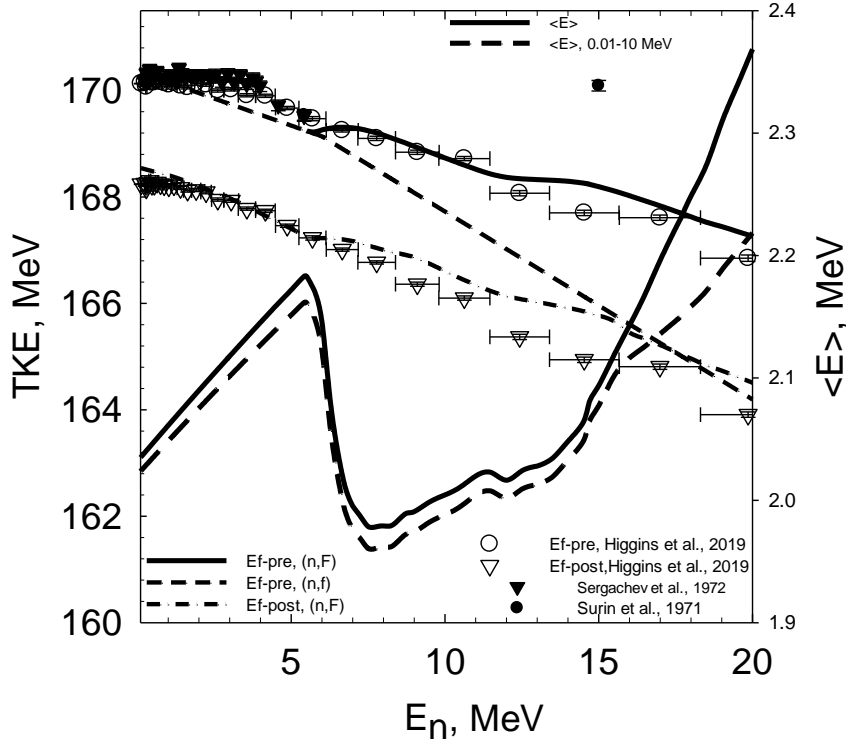


Fig.23. Total kinetic energy TKE: $^{233}\text{U}(n, F)$, E_F^{pre} — — —; $^{233}\text{U}(n, f)$, E_f^{pre} — — — —; $^{233}\text{U}(n, F)$, E_F^{post} — — — • — — —; \circ — $^{233}\text{U}(n, F)$, E_F^{pre} [43]; \blacktriangledown — $^{233}\text{U}(n, F)$, E_F^{pre} [47]; \bullet — $^{233}\text{U}(n, F)$, E_F^{pre} [48]; ∇ — $^{233}\text{U}(n, F)$, E_F^{post} [43]; — — — — —, — — — — — — $\langle E \rangle$ $^{233}\text{U}(n, F)$ in the range $\varepsilon \sim 0-20$ MeV и $\varepsilon \sim 0.01-10$ MeV, respectively.

$^{239}\text{Pu}(n, F)$ PFNS [13, 29, 31]. Figures 18 and 19 demonstrate partial contributions $\tilde{S}_{A+1}(\varepsilon, E_n)$, $\tilde{S}_A(\varepsilon, E_n)$, $\tilde{S}_{A-1}(\varepsilon, E_n)$ and $\tilde{S}_{A-2}(\varepsilon, E_n)$ for the observed PFNS of $^{235}\text{U}(n, F)$, $^{239}\text{Pu}(n, F)$ and $^{233}\text{U}(n, F)$ reactions at $E_n = 20$ MeV. The observed PFNS of $^{235}\text{U}(n, F)$ and $^{233}\text{U}(n, F)$ almost coincide, as do the contributions of $^{233}\text{U}(n, 2nf) — \tilde{S}_{232}(\varepsilon, E_n)$ and $^{235}\text{U}(n, 2nf) — \tilde{S}_{234}(\varepsilon, E_n)$. The lumped contribution of neutrons, emitted by fission fragments of $^{233}\text{U}(n, f) — \tilde{S}_{234}(\varepsilon, E_n)$, $^{233}\text{U}(n, nf) — \tilde{S}_{233}(\varepsilon, E_n)$ and $^{235}\text{U}(n, f) — \tilde{S}_{236}(\varepsilon, E_n)$, $^{235}\text{U}(n, nf) — \tilde{S}_{235}(\varepsilon, E_n)$ also almost coincide.

Observed PFNS of $^{233}\text{U}(n, F)$ and $^{239}\text{Pu}(n, F)$ are quite different, contribution of $^{233}\text{U}(n, f) — \tilde{S}_{234}(\varepsilon, E_n)$ in the vicinity of $\varepsilon \sim 1$ MeV is twice lower than the contribution of $^{239}\text{Pu}(n, f) — \tilde{S}_{240}(\varepsilon, E_n)$. Contributions of $^{233}\text{U}(n, nf) — \tilde{S}_{233}(\varepsilon, E_n)$ and $^{233}\text{U}(n, 2nf) — \tilde{S}_{232}(\varepsilon, E_n)$ in the vicinity of $\varepsilon \sim 1$ MeV is twice larger than the contributions of $^{239}\text{Pu}(n, nf) — \tilde{S}_{239}(\varepsilon, E_n)$ and $^{239}\text{Pu}(n, 2nf) — \tilde{S}_{238}(\varepsilon, E_n)$, respectively.

Average prompt fission neutron number

Average prompt fission neutron number $\nu_p(E_n)$ of $^{233}\text{U}(n,F)$ was measured in [59–71]. Partial average neutron numbers $\nu_{px}(E_{nx})$ define relative contributions of pre-fission neutrons with spectra $d\sigma_{n,xf}^k/d\varepsilon$ and prompt neutrons, emitted from fission fragments, $S_{A+2-x}(\varepsilon, E_n)$, see Eq. (2) and equations for $\tilde{S}_{A+2-x}(\varepsilon, E_n)$. To calculate $\nu_p(E_n)$ when $E_n > E_{nmf}$, the data on $\nu_p(E_n)$ for $^{233-x}\text{U}(n,F)$ at $E_n < E_{nmf}$ should be used, when available. The partial contributions to the PFNS are correlated with partial contributions of $\nu_p(E_n)$. Figure 20 compares the model calculation (Eq. (9)) with measured data. Partial contributions of $^{233}\text{U}(n,f)$, $^{233}\text{U}(n,nf)$ and $^{233}\text{U}(n,2nf)$ reactions are shown, as well as lumped contributions of $^{233}\text{U}(n,nf)^1$, $^{233}\text{U}(n,2nf)^{1,2}$ and $^{233}\text{U}(n,3nf)^{1,2,3}$, reactions, $\nu_{pre}(E_n)$, and post-fission neutrons, emitted from fission fragments, $\nu_{post}(E_n)$. Partial contribution of $^{233}\text{U}(n,nf)$ reaction influences but only weakly smooth energy dependence $\nu_p(E_n)$ around E_{nmf} threshold. The values of $\nu_{post}(E_n)$ and $\nu_{pre}(E_n)$ of $^{233}\text{U}(n,F)$ and $^{235}\text{U}(n,F)$ are influenced by values $\beta_x(E_n) = \sigma_{n,xf}/\sigma_{n,F}$ mostly (see Fig. 9).

Average energies of PFNS

Average energy of prompt fission neutron spectra is its rather rough signature. Figure 21 evidence that the shapes of $\langle E \rangle(E_n)$ in cases of $^{233}\text{U}(n,F)$ and $^{235}\text{U}(n,F)$ [23] are quite similar. Values of $\langle E \rangle$ [10] are presented here in the outgoing neutron energy interval $\varepsilon \sim 0.01$ –10 MeV. Our estimate of $\langle E \rangle(E_n)$ for $^{235}\text{U}(n,F)$ [23] reproduces the estimate of $\langle E \rangle$ based on measured PFNS data [11], especially around thresholds of $^{235}\text{U}(n,nf)$ and $^{235}\text{U}(n,2nf)$ reactions. Estimates of [10, 26, 28, 30] are discrepant with estimate of [23] in the interval $E_n \sim 8$ –10 MeV only.

The estimate of $\langle E \rangle(E_n)$ for the interval $\varepsilon \sim 0$ –20 MeV is shown on Fig. 22. Though the estimates of PFNS given in the data file of ENDF/B–VIII.0 [16] and JENDL–4.0 [17] predict some variation of $\langle E \rangle(E_n)$ for $^{235}\text{U}(n,F)$ at $E_n > E_{nmf}$, the correlation of these variations with the pre-fission (n,xf) neutrons might be considered imposed. In [16, 17] the correlation of observed PFNS shape with values of $\beta_x(E_n) = \sigma_{n,xf}/\sigma_{n,F}$, exclusive (n,xf)^{1...x} pre-fission neutron shapes is distorted or treated improperly (see Fig. 17). Present estimate of $^{233}\text{U}(n,F)$ PFNS $\langle E \rangle$ correlates with calculated shape of PFNS. The influence of $^{233}\text{U}(n,2nf)^{1,2}$ neutrons on $\langle E \rangle$ is much stronger than that of $^{239}\text{Pu}(n,2nf)^{1,2}$ in $^{239}\text{Pu}(n,F)$ reaction, while the fission cross sections values of $^{233}\text{U}(n,F)$ and $^{239}\text{Pu}(n,F)$ are quite similar. The correlation of $^{233}\text{U}(n,F)$ PFNS shape with $\langle E \rangle(E_n)$ produces $\langle E \rangle$ which is quite similar to $\langle E \rangle$ of $^{235}\text{U}(n,F)$ (see Fig. 21).

Average total kinetic energies of fission fragments TKE

Origin of local variations of TKE is due to (n,xf) reactions contributions to the observed fission cross section and its dependence on partial TKE of ^{234}U , ^{233}U , ^{232}U and ^{231}U fissioning nuclides on the excitation energy. The contribution of the (n,nf) reaction to the observed $\sigma_{n,F}$ of $^{233}\text{U}(n,F)$ reaction is much higher (see Fig. 8) than in case of $^{235}\text{U}(n,F)$ and $^{239}\text{Pu}(n,F)$ reactions (see Fig. 9), however, the local variations of TKE in $^{233}\text{U}(n,F)$ reaction are might be weaker.

The decrease of E_f^{pre} with the increase of the excitation energy while $E_n < E_{nnf}$, i.e. in the first-chance fission $^{233}\text{U}(n,f)$ domain [34], might be due to increase of the distance between fragments at the scission point, as proposed for $^{235}\text{U}(n,f)$ reaction [72]. However, for $^{233}\text{U}(n,f)$ reaction the decrease of TKE with increase of E_n is less evident. Local maxima in TKE at $E_n > E_{nnf}$, before and after prompt fission neutron emission, in the vicinity of $^{233}\text{U}(n,nf)$ and $^{233}\text{U}(n,2nf)$ reaction, were observed in [34]. Figure 23 shows that present estimate of TKE in $^{233}\text{U}(n,F)$ reaction correlates with $\langle E \rangle(E_n)$ of PFNS. The variation of TKE in the vicinity of (n,xnf) reaction thresholds due to decrease of excitation energy after pre-fission neutron emission helps to reproduce measured TKE of [34]. That peculiarity might be considered an indirect proof of calculated shape of PFNS around (n,xnf) thresholds, exclusive neutron $(n,xnf)^{l \dots x}$ pre-fission spectra and contributions of (n,xnf) reactions to the observed fission cross section of $^{233}\text{U}(n,F)$.

Contribution of (n,nf) reaction to the $\sigma_{n,F}$ of $^{233}\text{U}(n,F)$, is larger than contribution of $^{235}\text{U}(n,nf)$ to the fission cross section of $^{235}\text{U}(n,F)$, nonetheless the local bumps in TKE around $^{233}\text{U}(n,2nf)$ and $^{233}\text{U}(n,nf)$ reaction thresholds are weaker. That might be due to rather flat dependence on excitation energy of TKE for $^{232,233,234}\text{U}$, opposite to the case of TKE for $^{235,236,237,238,239}\text{U}$ fissioning nuclides [73, 74]. Contrary case is the TKE in $^{232}\text{Th}(n,F)$ reaction [35, 75]. It was observed that TKE of $^{232}\text{Th}(n,F)$ at $E_n < E_{nnf}$ increases. That peculiarity explains the occurrence of local minima in TKE in $^{232}\text{Th}(n,F)$ reaction [76–78]. To reproduce the observed dependence of E_f^{pre} on E_n in $^{233}\text{U}(n,F)$ reaction one may assume linear dependence of first-chance fission TKE $-E_{f0}^{pre}(E_n)$.

Conclusions

A number of observed peculiarities in PFNS, TKE, $\nu_p(E_n)$ correlate with the occurrence of pre-fission (n,xnf) neutrons, as predicted for the $^{233}\text{U}(n,F)$ and $^{233}\text{U}(n,xnf)$ and earlier for $^{235}\text{U}(n,F)$ and $^{235}\text{U}(n,xnf)$ [74]. Cross ratios of PFNS of $^{233}\text{U}(n,F)$, $^{235}\text{U}(n,F)$ and $^{239}\text{Pu}(n,F)$ reactions are compatible with measured data [11–13, 79]. The correlation of PFNS shape and emissive $((n,xnf))$ fission contribution to the observed fission cross section for $^{233}\text{U}(n,F)$ and $^{235}\text{U}(n,F)$ reactions. Spectra of pre-fission neutrons are rather soft as compared

with spectra of prompt neutrons emitted from fission fragments. The net effect of these peculiarities is the occurrence of dips in $\langle E \rangle$ in the vicinity of (n,nf) and $(n,2nf)$ reaction thresholds. Amplitude of dips in $\langle E \rangle$ of $^{233}\text{U}(n,F)$ PFNS is quite similar to that observed in PFNS of $^{235}\text{U}(n,F)$ reaction, notwithstanding the appreciable differences of $^{233}\text{U}(n,xnf)$ and $^{235}\text{U}(n,xnf)$ reaction contributions to the observed fission cross sections $^{233}\text{U}(n,F)$ and $^{235}\text{U}(n,F)$, respectively. That is explained by relatively large contributions of $v_{px}(E_{nx})$ as compared with $v_{pre}(E_n)$ for the reaction $^{233}\text{U}(n,F)$. In observed PFNS the partial components of (n,f) and (n,xnf) reactions are revealed. It might be argued that correct estimate of the exclusive pre-fission (n,xnf) neutron spectra and modelling of spectra of neutrons emitted from excited fission fragments gives a robust prediction of PFNS for $^{233}\text{U}(n,F)$ for incident neutron energies $E_n \sim E_{th} - 20$ MeV with a precision comparable to that of $^{235}\text{U}(n,F)$ PFNS.

References

1. *Zamyatnin Yu.S., Saphina I.N., Gutnikova E.K., Ivanova N.I.*—Atomnaya Energiya, 1958, vol. 4, № 4, P.337—342.
2. *Weisskopf W.F.*—Phys. Rev., 1937, vol. 52, P.295.
3. *Watt B.E.*— Phys. Rev., 1952, vol. 87, p. 1037.
4. *Maslov V. M., Baba M., Hasegawa A., Kagalenko A. B., Kornilov N.V., Tetereva N.A.*, INDC (BLR) -18, IAEA, Vienna (2003), <https://www-nds.iaea.org/publications/indc/indc-blr-0018/>
5. *Maslov V. M., Baba M., Hasegawa A., Kagalenko A. B., Kornilov N.V., Tetereva N.A.*, <https://www-nds.iaea.org/minskact>
6. *Starostov B.I., Nefedov V.N., Boytsov A.A.* — Vopr. At. Nauki Techn., Ser. Nucl. Const., 1985, № 3, c.16.
7. *Miura T, Baba M., Than Win, Ibaraki M., Hirasawa Y., Hiroishi T. and Aoki T.* — Journal of Nuclear Science and Technology, 2002, vol.39, p. 409.
8. *Vorobyev A.S., Shcherbakov O.A.*—Vopr. At. Nauki Techn., Ser. Nucl. Const., 2016, № 2, P.52.
9. *Vorobyev A.S., Shcherbakov O.A.*, Vopr. At. Nauki Techn., Ser. Nucl. Const., 2011-2012, № 1-2, P.37.
10. *Maslov V.M., Pronyaev V.G., Tetereva N.A. et al.*—Proc. Intern. Conf. Nuclear Cross Sections and Technology, Jeju, Korea, 2010, Journal of Korean Phys. Soc., 2011, vol. 59, p. 1337.
11. *Kelly K. J., Gomez J.A., Devlin M. et al.*—Phys. Rev. C, 2022, vol. 105, p. 044615.
12. *Kelly K. J., Devlin M., O'Donnell J.M. et al.*—Phys. Rev. C, 2020, vol. 102, p. 034615.
13. *Marini P., Taieb J., Laurent B. et al.*—Phys. Rev. C, 2020, vol. 101, p. 044614.
14. *Chadwick M., M. Herman, P. Oblozinsky et al.* —*Nuclear Data Sheets*, 2011, vol. 112, p. 2887-2996.

15. OECD/NEA. JEFF—3.3 Evaluated Data Library. Neutron data. Technical Report, 2018.
16. **Brown D. A., Chadwick M. B., Capote R. et al.**—Nuclear Data Sheets, 2018, vol. 148, p. 1.
17. **Shibata K., Iwamoto O., Nakagawa T. et al.**—J. Nucl. Sci. Technol., 2011, vol. 48, p. 1.
18. **Zabrodskaya S.V., Ignatyuk A.V., Koscheev V.N. et al.** — Vopr. At. Nauki Techn., Ser. Nucl. Const., 2007, № 1-2, P.3.
19. **Blokhin A.I., Gai E.V., Ignatyuk A.V. et al.**— Vopr. At. Nauki Techn., Ser. Nucl. Const., 2016, № 2, P.62.
20. **Johansson P., Holmqvist B., Wiedling T. et al.**—In: Proc. Intern. Conf. on Nuclear Cross Sections and Technology. Washington, 1975, vol. 2, p. 572—575.
21. **Staples P., Egan J.J., Kegel G.H.R. et al.** — Nucl. Phys. 1995, vol. A591, p. 41—55.
22. **Lovchikova G.N., Smirenkin G.N., Trufanov A.M. et al.**—Yadernaya Fyzyka, 1999, vol. 62, P.1551—1561.
23. **Maslov V.M.**, —LXXII International conference “Nucleus-2023”, Fundamental Problems and applications, Moscow, July, 11–16, 2022, Book of Abstracts, p.111, https://events.sinp.msu.ru/event/8/attachments/181/875_nucleus-2022-book-of-abstracts-www.pdf.
24. **Kornilov N.V., Kagalenko A.B., Hamsch F.-J.** — Yadernaya Fyzyka, 1999, vol. 62, c.209.
25. Fission neutron Spectra of Uranium-235, NEA, NEA/WEC-9, OECD, 2003.
26. **Maslov V.M., Kornilov N.V., Kagalenko A.B., Tetereva N.A.**—Nucl. Phys. A, 2005, vol. 760, p. 274,
27. **Maslov V.M., Porodzinskij Yu. V., Baba M., Hasegawa A., Kornilov N.V., Kagalenko A.B. and Tetereva N.A.**— Phys. Rev. C, 2004, vol. 69, p. 034607.
28. **Maslov V.M., Kornilov N.V., Kagalenko A.B., Tetereva N.A.**, <https://www-nds.iaea.org/minskact/data/92235f18.txt>.
29. **Maslov V.M.**—Atomnaya Energiya, 2007, vol.103, P.119.
30. **Maslov V.M., Tetereva N.A., Pronyaev V.G. et al.**—Atomnaya Energiya, 2010, vol. 108, P.352.
31. **Maslov V.M.**—Vopr. At. Nauki Techn., Ser. Nucl. Reactors., 2006, № 2, P.33, http://vniief.ru/wps/wcm/connect/vniief/site/publishing/publications/nuclearreactor/y2006/y2-2006/vipusk2_2006.
32. **Maslov V.M.**—Yadernaya Fyzyka, 2008, vol. 71, P.11.
33. **Madland D.**—Nucl. Phys. A, 2006, vol. 772, p. 113.
34. **Higgins D., Greife U., Tovesson F., Manning B., Mayorov D., Mosby S., Schmitt K.** —Phys. Rev. C, 2020, vol. 101, p. 014601.
35. **Maslov V.M.** <http://isinn.jinr.ru/past-isinns/isinn-27/abstracts/Maslov.pdf>
36. **Duke D.L., Tovesson F., Brys T. et al.**—Proc. Intern. Conf. Nuclear Data for Science and Technology, Bruges, Belgium, September 11—16, 2016, A.Plompen, et al, Ed. p. 04042, (2017); Eur. Phys. Journ. Web of Conf., 2017, vol. 146, 04042.
37. **Yanez R., Loveland W., King J., Barrett J.S., Fotiades N., Lee H.Y.**—Nucl. Phys.

- A, 2018, vol. 970, p. 65.
38. **Dyachenko P.P., Kuzminov B.D., Tarasko M.Z.**, —Yadernaya Fyzyka, 1968, vol. 8, P.286.
 39. **Surin V.M., Sergachev A.I., Rezhikov N.I.**—Yadernaya Fyzyka, 1968, vol. 14, P.935.
 40. **Meierbachtol K., Tovesson F., Duke D. L. et al.**— Phys. Rev. C , 2016, vol. 94, 034611.
 41. **Chemey A., Pica A., Liangyu Yao, Loveland W., Hye Young Lee, Kuvin S.A.**—The European Physical Journal A, 2020, vol. 56, p. 297.
 42. **Maslov V.M. and Kikuchi Ya.**—Nuclear Science and Engineering, 1996, vol. 124, p. 492.
 43. **Fursov B.I., Kupriyanov V.I., Smirenkin G.N.**— Atomnaya Energiya, 1978, vol. 44, P.236.
 44. **Calviani M., Praena J., Abbondanno U. et al.**— Phys. Rev. C, 2009, vol. 80, 044604.
 45. **Kalinin V.A., Kovalenko S.S., Kuzmin V.N. et al.**—Vopr. At. Nauki Techn., Ser. Nucl. Const., 1987, № 4, c.3. 1987.
 46. **Adamov V.M., Aleksandrov B.M., Alkhozov I.D.**— Vopr. At. Nauki Techn., Ser. Nucl. Const., 1977, №24, c.8-15.
 47. **Alkhozov I.D., Ganza E.A., Drapchinsky L.V.** —In: Proc. III All-Union workshop on metrology of neutron beam in reactors and accelerators. Moscow, 1982., 1983, P. 201.
 48. **Scherbakov O.A., Donets A.Yu., Evdokimov A.V., Fomichev A.V., Fukahori T., Hasegawa A., Laptev A.B., Maslov V.M., Petrov G.A., Tuboltsev Yu.V., Soloviev S., Vorobyev A.S.** —Proc. of International Conference on Nuclear Data for Science and Technology, October 7-12, 2001, Tsukuba, Japan, p. 230, 2002.
 49. **Carlson G.W., Behrens J.W.** — Nucl. Sci. Eng., 1978, vol. 66, p. 205.
 50. **Zasadny K.R., Agrawal H.M., Mahdavi M., Knoll G.F.** — Trans. Amer. Nucl. Soc. 1984, vol. 47, p.425.
 51. **Tovesson F., Laptev A., Hill T.S.**— Nucl. Sci. Eng., 2014, vol. 178, p. 57.
 52. **Lisowski P.W, Gavron A., Parker W.E., Balestrini A.D., Carlson, Wasson O.A., Hill N.W.**—Proc. of International Conference on Nuclear Data for Science and Technology, May, 1991, Julich Germany, p. 732, 1991.
 53. **Belloni F., Calviani M., Colonna N. et al.**— Europ. Phys. Journ. A, 2011, vol. 47, p. 2.
 54. **Maslov V.M.**— Phys. Rev.C, 2005, vol. 72, 044607.
 55. **Maslov V.M.**, LXXII International conference “Nucleus-2023”, Fundamental Problems and applications, Moscow, July, 11–16, 2022, Book of Abstracts, 11–16, 2022, Book of Abstracts, p.168,
https://events.sinp.msu.ru/event/8/attachments/181/875_nucleus-2022-book-of-abstracts-www.pdf.
 56. **Maslov V.M., Porodzinskij Yu.V., Tetereva N.A. et al.**—Nucl. Phys. A, 2006, vol. 764, p. 212.
 57. **Kelly K. J., Kawano T., O'Donnel J.M. et al.**—Phys. Rev. Lett., 2019, vol. 122, p. 072503.
 58. **Boykov G.S., Dmitriev V.D., Kudyaev G.A., et al.** —Yadernaya Fyzyka, 1991, vol. 53, P.628.
 59. **Hopkins J.C., Diven B.C.**— Nucl. Phys., 1963, vol. 48, p. 433.
 60. **Gwin R., Spencer R.R. and Ingle R.W.** — Nucl. Sci. Eng., 1986, vol. 94, p. 365.

61. **Mather D.S., Fieldhouse P. and Moat A.** —Nucl. Phys., 1965, vol. 66, p. 149.
62. **Walsh R.L. and Boldeman J.W.**— Journal of Nucl. Energy, 1971, vol. 25, p. 321.
63. **Nurpeisov B., Nesterov V.G., Prokhorova L.I. et al.** — Atomnaya Energiya,1973, vol. 34, P.491.
64. **Nurpeisov B., Volodin K.E., Nesterov V.G. et al.**— Atomnaya Energiya,1975, vol. 39, P.199.
65. **Sergachev A.I., Dyachenko P.P., Kovalev A.M., Kuzminov B.D.,**—Yadernaya Fyzyka, 1972, vol. 16, P.475.
66. **Johnstone I.** AERE 1912, 1956.
67. **Colvin D.W., Sowerby M.G.,** Prompt neutron yield determination for U-233 neutron induced fission, BNL-325.
68. **Smirenkin G.N., Bondarenko I.I., Kutsaeva L.S. et al.** — Atomnaya Energiya,1958, vol. 4, P.188.
69. **Kolosov N.P., Kuzminov B.D., Sergachev A.I., Surin V.M.** — Atomnaya Energiya,1972, vol. 32, P.83.
70. **Protopopov A.N., Blinov M.V.**— Atomnaya Energiya,1958, vol. 5, P.71.
71. **Flerov G.N. , Talyzin V.M.**— Atomnaya Energiya,1961, vol. 10, P.68.
72. **Shimada K., Ishizuka Ch., Ivanyuk F. A. et al.**— Phys. Rev. C, 2021, vol. 104, p. 054609.
73. **Maslov V.M.,** Physics of Particles and Nuclei Letters 20 (4), 565-576, 2023; <https://link.springer.com/article/10.1134/S1547477123040490>
74. **Maslov V.M.,** Physics of Atomic Nuclei, 2023, Vol. 86, No. 5, pp. 627–669. <https://www.pleiades.online/cgi-perl/search.pl?type=abstract&name=nuclphys&number=5&year=23&page=627;>
75. **Maslov V.M.,** 29th International Seminar on Interaction of Neutrons with Nuclei: May 29 - June 2, 2023, Frank' LNP, JINR, Dubna, Russia. http://isinn.jinr.ru/proceedings/isinn-29/pdf/Maslov_2r.pdf
76. **Goverdovsky A.A., Kuzminov B.D., Mitrofanov V.F., Sergachev A.I.,** Proc. Conf. on Nucl. Data for Sci. and Technol., Mito. 1988 p. 695.
77. **King J., Loveland W., Barrett J. S. et al.,** Eur. Phys. Journ. A, 53, 238 (2017).
78. **Higgins D., Greife U., Tovesson F. et al.,** Phys. Rev. C, 101, 014601 (2020).
79. **Devlin M., Bennett E. A., Buckner M. Q., et al.** In: Proceedings of the *International Conference Nuclear Data for Science and Technology, 24–29 July 2022, Sacramento, USA*; Eur. Phys. Journ. Web of Conf., 2023, v. 284, 04007.